The Journal of Experimental Biology 206, 2803-2829

doi:10.1242/jeb.00501

Dynamic flight stability in the desert locust *Schistocerca gregaria*

Graham K. Taylor* and Adrian L. R. Thomas

Department of Zoology, Oxford University, Tinbergen Building, South Parks Road, Oxford, OX1 3PS, UK

*Author for correspondence (e-mail: graham.taylor@zoo.ox.ac.uk)

Accepted 16 May 2003

Summary

Here we provide the first formal quantitative analysis of dynamic stability in a flying animal. By measuring the longitudinal static stability derivatives and mass distribution of desert locusts *Schistocerca gregaria*, we find that their static stability and static control responses are insufficient to provide asymptotic longitudinal dynamic stability unless they are sensitive to pitch attitude (measured with respect to an inertial or earth-fixed frame) as well as aerodynamic incidence (measured relative to the direction of flight). We find no evidence for a 'constant-lift reaction', previously supposed to keep lift production constant over a range of body angles, and show that such a reaction would be inconsequential because locusts can potentially correct for pitch disturbances within a single wingbeat. The static stability derivatives identify three natural longitudinal modes of motion: one stable subsidence mode, one unstable divergence mode, and one stable oscillatory mode (which is present with or without pitch attitude control). The latter is identified with the short period mode of aircraft, and shown to consist of rapid pitch oscillations with negligible changes in forward speed. The frequency of the short period mode (approx. 10 Hz) is only half the wingbeat frequency (approx. 22 Hz), so the mode would become coupled with the flapping cycle without adequate damping. Pitch rate damping is shown to be highly effective for this purpose – especially at the small scales associated with insect flight – and may be essential in stabilising locust flight. Although having a short period mode frequency close to the wingbeat frequency risks coupling, it is essential for control inputs made at the level of a single wingbeat to be effective. This is identified as a general constraint on flight control in flying animals.

Key words: stability, control, flapping flight, desert locust, *Schistocerca gregaria*, insect, flight dynamics, modes of motion, equations of motion, frequency response, stabilising pitch reaction, constant-lift reaction, flight speed, body angle.

Introduction

The insect flight literature still lacks a quantitative empirical analysis of stability and control in terms of its flight mechanics. Many previous studies have correlated changes in the aerodynamic forces or moments on tethered insects with changes in wing kinematics during fictive manoeuvres (for a review, see Taylor, 2001), but the measured force systems have almost always been incomplete in the sense of being insufficient to specify the direction, magnitude and line of action of the resultant force. Some studies (e.g. Weis-Fogh, 1956b; Cloupeau et al., 1979) have only measured the force in a single direction. Others (e.g. Thüring, 1986; Eggers et al., 1991) have measured the turning moment about one or more axes, but have not measured the forces normal to these axes (but for an exemplary exception, see Blondeau, 1981). A few studies (e.g. Wilkin, 1990) have measured both the direction and magnitude of the resultant force but not defined its line of action (but for a prescient exception, see Hollick, 1940). Of these studies, almost all have failed to record the centre of mass, which plays an analogous role in flight dynamics to the fulcrum in a game of seesaw.

These limitations have made it impossible to predict even the initial direction of a turn induced by a measured change in the forces, with the result that we still lack any quantitative empirical understanding of the stability of flying insects. An initial directional tendency to return to equilibrium after a disturbance is called static stability, which qualifies the fact that the dynamics of a system may prevent it from actually settling back to equilibrium. This means that even if we could measure an insect's initial turning tendency in response to a disturbance (i.e. measure its static stability), this would still be insufficient to say anything about the more interesting problem of dynamic stability without a formal theoretical framework for analysing the flight dynamics. Analyses of static stability in gliding animals (Thomas and Taylor, 2001; McCay, 2001) and flapping flight (Taylor and Thomas, 2002) have been provided elsewhere. Here we analyse the longitudinal flight dynamics of locusts empirically, providing the first formal framework for analysing the dynamic stability of flying animals. Our strategy parallels the engineering approach of measuring how the aerodynamic forces and moments change

with attitude and velocity in a wind tunnel, in order to define the parameters of the linearized equations of motion. Writing these equations enables us to use techniques of eigenvalue and eigenvector analysis to provide the first formal description of dynamic stability in a flying animal.

A formal framework for analysing *Animal flight stability*

The framework that we use is founded upon the linearized equations of rigid body motion, which are widely used in aircraft flight dynamics (e.g. Etkin and Reid, 1996; Boiffier, 1998) and have recently been used in approximate (Taylor and Thomas, 2002) or reduced form (Deng et al., 2002; Schenato et al., 2002) in theoretical considerations of animal flight dynamics. The framework is developed fully in the Appendix, but can be treated as a 'black box' if required (Fig. 1). Its single most important assumption is that the animal has only the 6 degrees of freedom of a rigid flying body: 3 in translation and 3 in rotation. This means dropping the wings' degrees of freedom relative to the body from the explicit formulation, so that although in reality the centre of mass moves and the forces, moments and moments of inertia change through every wingbeat, all are assumed to average out to make a constant contribution for a given flight configuration. Conceptually, the aerodynamic forces resulting from the flapping motion of each wing are collapsed into a single force vector, which may vary with speed and attitude to reflect changes in the wing kinematics with respect to the body as well as with respect to the air. These approximations are all reasonable if the wings beat fast enough not to excite the natural oscillatory modes of the system (Taylor and Thomas, 2002). In addition, the rigid body equations of motion contain no gyroscopic terms, which is reasonable because the combined mass of the oscillating wings is small (<4% of total body mass).

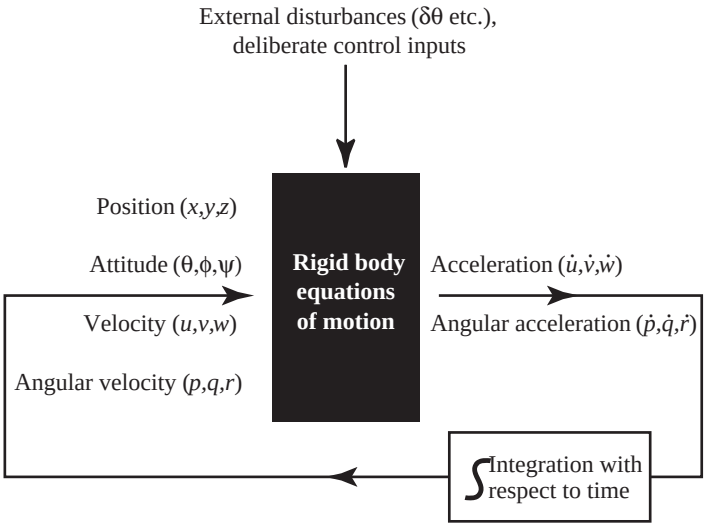

Fig. 1. Black box representation of the rigid body equations of motion underpinning the quantitative framework of this analysis. The integral sign represents a bank of single integrators.

Provided there exists a longitudinal plane of symmetry, pure longitudinal or symmetric motions are possible. This means that we can consider longitudinal dynamic stability in isolation from lateral dynamic stability, so we need only consider three of the animal's six degrees of freedom in the present analysis (Fig. 2). The rigid body equations of motion are intrinsically non-linear, but may be linearized by approximating the body's motion as a series of small disturbances from a steady, symmetric reference flight condition, and retaining only the linear terms in the Taylor series expansion. This yields a set of time (t) dependent equations, summarised by the expression:

$$\delta\dot{\mathbf{x}}_{\mathrm{sym}}(t) = \mathbf{F}_{\mathrm{sym}}\delta\mathbf{x}_{\mathrm{sym}}(t) + \mathbf{C}_{\mathrm{sym}}\delta\mathbf{c}_{\mathrm{sym}}(t)\,, \qquad (1)$$

for symmetric longitudinal motion (subscript 'sym'). Here $\mathbf{x}_{\mathrm{sym}}(t)$ is the longitudinal state vector $[u\ w\ q\ \theta]^{\mathrm{T}}$, containing the longitudinal state variables (Fig. 2): forward (u) and dorso-ventral (w) components of velocity along the x- and z-axes, the angular pitch rate at the centre of mass (q), and the pitch angle between the x-axis and the horizontal (θ). $\mathbf{F}_{\mathrm{sym}}$ is the longitudinal system matrix, containing partial derivatives of the longitudinal forces and moments with respect to the longitudinal state variables: the stability derivatives. $\mathbf{C}_{\mathrm{sym}}$ is the control system matrix, and has as many rows and columns as the number of symmetric control inputs available to populate the control state vector $\mathbf{c}_{\mathrm{sym}}$. Since the system matrices $\mathbf{F}_{\mathrm{sym}}$ and $\mathbf{C}_{\mathrm{sym}}$ contain only (real) constant numbers, Equation 1 is linear time-invariant with respect to disturbances from the equilibrium condition about which the equations are linearized.

Although the usual practice in the aircraft literature is to place aerodynamic effects arising from pilot and automatic control in $\mathbf{C}_{\mathrm{sym}}$ and to reserve $\mathbf{F}_{\mathrm{sym}}$ for passive aerodynamic effects, it is sometimes helpful to view automatic control as augmenting the stability derivatives in $\mathbf{F}_{\mathrm{sym}}$ (Etkin and Reid, 1996). We must use the latter approach here, because it is impossible to isolate the passive aerodynamic stability of a flapping insect without abolishing all of the control inputs that provide the feedback necessary for stimulating normal forward flight. The stability derivatives then conflate passive

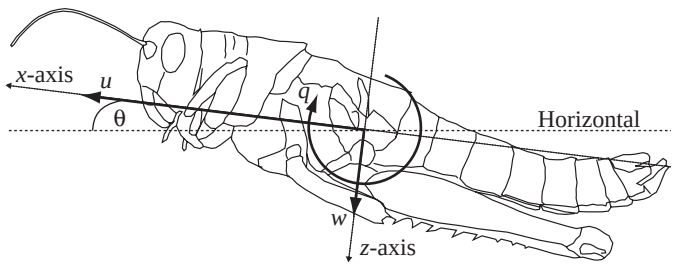

Fig. 2. Definition of the state variables u, w, q and θ. Each of the variables is signed positive in the direction shown. The body axes are centred upon the centre of mass and are aligned so that the x-axis points in the direction of flight at equilibrium. The locust is shown during a nose-up perturbation: q is zero at equilibrium, and w and θ are defined so as to be zero at equilibrium.

aerodynamic effects with aerodynamic effects arising from 'automatic' changes in muscle firing due to changes in body angle, wind speed, etc. The longitudinal system matrix $\mathbf{F}_{sym}$ containing these derivatives is written:

$$\mathbf{F}_{sym} = \begin{bmatrix} \frac{X_u}{m} & \frac{X_w}{m} & \frac{X_q}{m} - w_e & -\boldsymbol{g}\cos\theta_e \\ \frac{Z_u}{m} & \frac{Z_w}{m} & \frac{Z_q}{m} + u_e & -\boldsymbol{g}\sin\theta_e \\ \frac{M_u}{I_{yy}} & \frac{M_w}{I_{yy}} & \frac{M_q}{I_{yy}} & 0 \\ 0 & 0 & 1 & 0 \end{bmatrix} \quad (2)$$

where the terms (X_u, Z_u, M_u), (X_w, Z_w, M_w), (X_q, Z_q, M_q) denote partial derivatives of the forward (X) and dorso-ventral (Z) components of force and the pitching moment (M) about the centre of mass, with respect to the motion variables u, w and q, measured during tethered flight. The terms m and I_{yy} denote the reference body mass and pitching moment of inertia; u_e, w_e, θ_e denote values of the longitudinal state variables at equilibrium; $\boldsymbol{g}$ is the acceleration due to gravity ($\boldsymbol{g}$=9.81 m s^{-2}). We have dropped partial derivatives with respect to accelerations and angular accelerations, but Equation 2 is otherwise rather general. Similar equations can be found in any textbook on flight dynamics, whether for fixed-wing aircraft (e.g. Nelson, 1989; Etkin and Reid, 1996; Cook, 1997), helicopters (e.g. Padfield, 1996), airships (e.g. Khoury and Gillett, 1999), or spacecraft (e.g. Bryson, 1994). The differences between animals and aircraft are instead manifested in the stability derivatives determining the system's response to perturbation.

Materials and methods

The partial derivatives in the system matrix $\mathbf{F}_{sym}$ (Equation 2) can be empirically defined by measuring the changes in the forces and moments induced by imposed changes in velocity or orientation away from an equilibrium flight condition. This can only be done under open-loop conditions, where the insect is immobilised such that changes in the stroke cycle do not affect the external stimuli that the insect receives. We must therefore assume that the insect responds similarly to (instantaneously) identical perturbations from equilibrium in both the open-loop conditions of tethered flight and the closed-loop conditions of free flight. The slopes of linear regressions fitted to the open-loop data can then be used to provide direct estimates of the stability derivatives for populating the system matrix. This is the general strategy used to measure the stability derivatives in wind tunnel studies on aircraft, helicopters, airships, submarines and spacecraft. Here we extend it to flying animals.

Animals

Three adult male gregarious phase desert locusts *Schistocerca gregaria* Forskål were drawn from a population that had been reared in crowded laboratory culture in Oxford University's Zoology Department for 13 years. The small sample size was imposed by the difficulty of finding individuals that would fly reliably for the full 2–3 h required for each experiment, but is identical to that of previous studies (e.g. Zarnack and Wortmann, 1989) and is justified on the basis of the complexity of the analysis, which must be performed separately for each individual. The individuals are called 'R' (Red), 'G' (Green), and 'B' (Blue), and the data are colour coded in subsequent figures. Relaxed selection and inbreeding depression are expected to have lowered the mean flight performance of the population, so individuals were chosen on the basis of flight ability. Locusts were only picked if their wings and appendages were in perfect condition. Each individual was also checked for dynamically stable free flight performance by releasing it from an indoor balcony prior to the experiment.

Tethering

Each locust was rigidly tethered to a 6-component aerodynamic force balance (I-666, FFA Aeronautical Research Institute of Sweden) in a low speed, low turbulence, open-circuit wind tunnel (Fig. 3) designed specifically for insect flight work (G. K. Taylor and A. L. R. Thomas, manuscript in preparation). During steady flight the locusts made no attempt to grasp the tether, which consisted of a 0.5 mm sheet aluminium platform set upon a brass M2 screw and cemented with cyanoacrylate adhesive to the fused sternal sclerites forming the plastron of the pterothorax. This arrangement ensured that the angle of the force balance back from the vertical equated with the body angle (α_b), defined by Weis-Fogh (1956a) as the angle between the oncoming wind and the plastron.

Force measurements

The force balance was sting-mounted to a rotary stage (Edmund Industrial Optics, Barrington, NJ, USA) providing repeatable pitch adjustment $0°\leq\alpha_b\leq14°\pm0.5°$. Force transduction was by foil strain gauges in full Wheatstone bridge configuration, with 5 mA constant current excitation provided by a 6-channel bridge amplifier (2210A Signal Conditioning Amplifier/2250A Rack Adapter, Vishay Measurements Group, Raleigh, NC, USA). Each output was filtered online with a 1 kHz low-pass hardware filter (4th order Chebyshev), sampled at 10 kHz using a 16-bit analogue-to-digital converter (Maclab 8s, ADInstruments, Pty Ltd., Castle Hill, NSW, Australia), and recorded using 12 bits in Chart 3.6/s (AD instruments 1998) on an Apple 9600 PowerMac.

Flight conditions

Standard conditions of 29±1°C temperature and 35±5% relative humidity were maintained throughout the experiments. To give reliable flight performance, we used diffuse overhead low-level (20 lux) red lighting (Weis-Fogh, 1956a) provided by light from a red-filtered 250 W slide projector. Blackout

cloth prevented light entering the sides of the tunnel, and the room was kept in darkness to minimise extraneous visual input. The locusts initially attempted to escape from the tether, displaying pronounced deflections of the abdomen that are normally associated with avoidance manoeuvres (for a review, see Taylor, 2001). Measurements were made only when the locust had settled into flying in the complete flight posture, defined by Weis-Fogh (1956a) as when "*the antennae are stretched obliquely forwards, the forelegs are drawn up, the middle legs and the hind femora are stretched backwards along the abdomen, the hind tibiae are drawn up against the shallow groove on the underside of the femora, and the abdomen points straight backwards in continuation of the pterothorax*" (p. 463). The transition to this posture was accompanied by a switch to a very regular and pulse-like lift trace, with no unbalanced side forces and roll or yaw moments. Once adopted, the complete flight posture tended to be assumed for the duration of the experiments, which lasted between 2 and 3 h, including a further 10 min for the locust to settle into steady flight at the reference speed (U_{ref}=3.50 m s^{-1}) and reference body angle ($\alpha_{b,ref}$=7°): values previously found to stimulate tethered flight with lift balancing body weight (Weis-Fogh, 1956a,b; Zarnack and Wortmann, 1989; Wortmann and Zarnack, 1993).

Flight experiments

Each experiment comprised two consecutive measurement series: an angle series, in which α_b was varied whilst tunnel speed U was fixed at U_{ref}, and a speed series, in which U was varied whilst α_b was fixed at $\alpha_{b,ref}$. The ranges for U and α_b were within those observed in cruising and climbing natural free flight for *Schistocerca gregaria* (Waloff, 1972) and *Locusta migratoria* L. (Baker et al., 1981). The angle series comprised 14 pairs of force measurements lasting 13 s each, made first at a perturbed angle $0°\leq\alpha_b\leq14°$ and then at $\alpha_{b,ref}$ within the same minute. We alternated between perturbed angles higher and lower than $\alpha_{b,ref}$ to avoid correlating any systematic effect of time with α_b. For each pair of measurements, we subtracted the forces measured at $\alpha_{b,ref}$ from those measured at the perturbed body angle to remove the temporal variation in flight performance that has beset previous studies (e.g. Zarnack and Wortmann, 1989). We then added the mean of the 14 measurements at $\alpha_{b,ref}$ to reconstruct an absolute value of force production. The speed series comprised eight measurements made over a range of speeds ($2.00\leq U\leq5.00$ m s^{-1}), beginning and ending with U_{ref}. Each measurement lasted approximately 13 s, and we alternated between speeds higher and lower than U_{ref} to avoid correlating any systematic effect of time with U. This procedure is important because it ensures that temporal variation in flight performance cannot introduce systematic bias into our estimates of the stability derivatives. The speed series measurements were necessarily unpaired to avoid completely fatiguing the locust.

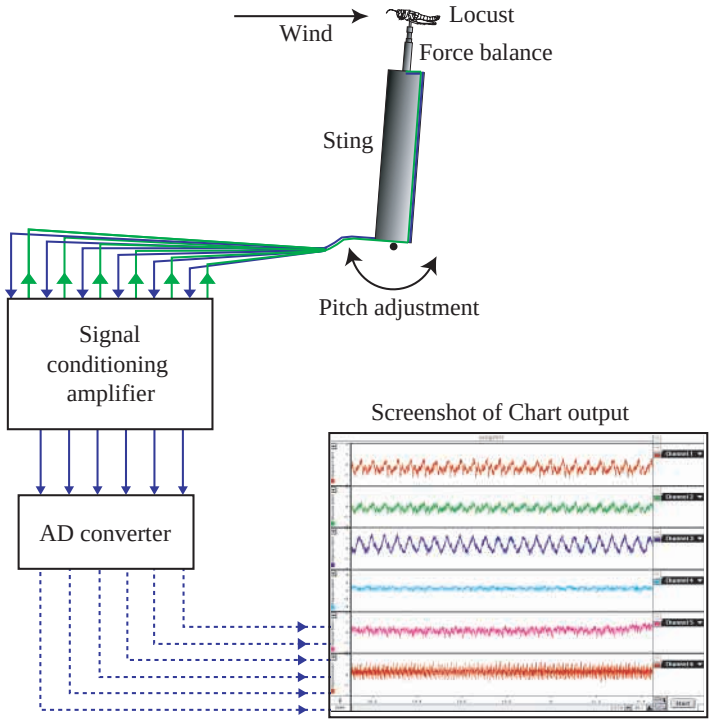

Fig. 3. Schematic representation of the experimental setup. AD, analogue-to-digital.

Conversion of balance output to dimensionless force–moment data

Each force-balance recording was trimmed in Chart to contain an integer number of complete stroke cycles (typically around 250). Subsequent analysis was performed using custom-written programmes in Matlab 5.2.1 (1998; The Mathworks Inc., Natick, MA, USA) on an Apple G4 PowerMac. A number of extraneous factors affect balance output: amplifier zeroes drift with temperature, and bridge resistance changes with balance orientation. Corrections were applied to remove these effects, and will be described in detail elsewhere (G. K. Taylor and A. L. R. Thomas, in preparation). The corrected balance output was converted to force–moment units using a static calibration analysed as a General Linear Model (GLM), in which we retained significant terms up to third order in any one channel plus all significant second order interactions ($P\leq0.05$; G. K. Taylor and A. L. R. Thomas, in preparation). We then took the mean of each force–moment measurement, subtracted the gravitational forces and moments due to the locust and its tether, and resolved the forces at the centre of mass. Drag on the tether was estimated using a standard empirical formula for a cylinder (White, 1974), but was sufficiently small to be ignored. For convenience and ease of comparison with the existing literature, we resolved the resultant aerodynamic force on the locust into an upward component ('lift') and a forward component (called 'thrust–drag' to indicate that it is equivalent to thrust minus drag, although the two were never separated). The forces were normalised by reference body weight, which is consistent with the form of Equation 2 and allows the dimensionless forces to be compared directly with each

Table 1. *Morphometric measurements for the three locusts*

Locust	Reference body mass (g)	Reference body length (mm)	Forewing length (mm)	Hindwing length (mm)	Combined forewing mass (g)	Combined hindwing mass (g)
'R'	1.8490	46.0	49.1	44.2	0.0418	0.0338
'G'	1.4357	40.5	44.1	40.7	0.0339	0.0237
'B'	1.8610	46.0	47.9	44.5	0.0355	0.0279

other. The pitching moment about the centre of mass was made dimensionless by dividing through by the product of reference body weight and length. These dimensionless quantities are henceforth referred to as 'relative lift' (L_r), 'relative thrust–drag' (T_r) and 'relative pitching moment' (M_r), following the notation of Weis Fogh (1956a).

Morphometric measurements

Morphometric measurements are given in Table 1. Each locust was weighed at the beginning and end of the experiment, and was then frozen in a sealed container at –40°C. Reference body mass was defined as the mass of the locust at the mean time of force measurement, assuming linear loss of mass with time. Reference body length was measured from the frons to the tip of the abdomen using a pair of electronic callipers (Absolute Digimatic, Mitutoyo Corporation, Kawasaki, Kanagawa, Japan); reference wing length was measured from wing base to wing tip.

Centre of mass measurements

The locusts were later defrosted and fixed in the complete flight posture using tiny amounts of cyanoacrylate adhesive. The centre of mass was determined using a model aircraft propeller balancer (Precision Magnetic Balancer, Top-Flite, Hobbico Inc., Champaign, Il, USA), which uses powerful magnets to levitate a steel shaft under almost frictionless conditions. Balanced stays were used to hang the locust from the shaft so that its centre of mass always hung vertically below the shaft axis. Plumb lines were hung on either side of the locust for sighting purposes, and were aligned in the viewfinder of a Canon XL1 Camcorder. We were later able to overlay left–right pairs of camcorder images and use the intersection of the plumblines to determine the position of the centre of mass (Fig. 4). Measurements agreed to better than ±1 mm between the three locusts (approximately 2% of body length). The wings comprise <4% of total body mass, so the centre of mass is expected to vary little through the wingbeat.

Calculation of pitching moment of inertia

The body's pitching moment of inertia was approximated by sectioning the frozen body of each locust into eight transverse sections of equal thickness (Fig. 5B). The mass of each section (expressed as a percentage of total frozen body mass) was then averaged across the three locusts (Fig. 5A). The lateral projected area of each section was measured in NIH Image 1.62 and expressed as a percentage of the total lateral projected area of the locust. Each section was then approximated as a rectangle of equivalent width and area, located with its centre of area vertically coincident with the centre of area of the section (Fig. 5C). The relative density (σ_i) of each rectangle i (mean percentage mass over mean percentage area) is represented in Fig. 5C by the density of shading. The dimensionless contribution of each rectangle to I_{yy} is then:

$$\iint \sigma_i(\hat{x}^2 + \hat{z}^2)\mathrm{d}\hat{x}\mathrm{d}\hat{z}\,, \qquad (3)$$

evaluated over the area of the rectangle, where $\hat{x}$ and $\hat{z}$ are dimensionless coordinates in the body axes, normalised by body length. The total pitching moment of inertia is the sum of the eight contributions multiplied by $m_b l^4/a$ for each locust,

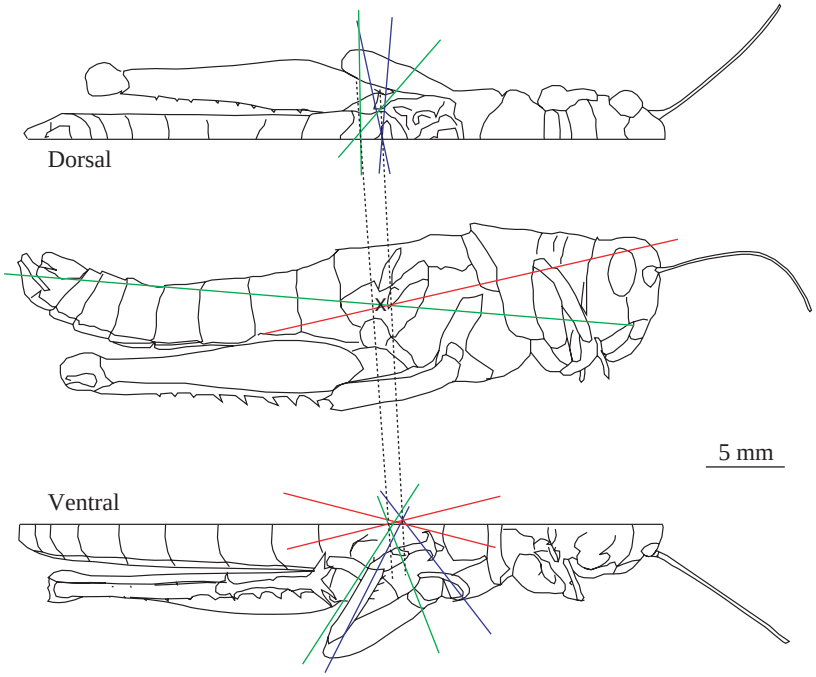

Fig. 4. Centre of mass measurements. Dorsal, lateral and ventral views of a locust, showing the average position of the centre of mass (x). The line drawings were traced from images generated by placing locust 'G' directly onto a flatbed scanner, and are scaled accordingly. Plumb lines passing through the centre of mass are shown as coloured lines, with the colours denoting the locust from which they were obtained (red 'R', green 'G', blue 'B'). The intersection of the plumb lines corresponds to the position of the centre of mass; dotted lines join the most forward and rearward plumb line intersections on the dorsal and ventral views to give an indication of measurement error.

where m_b is the reference body mass less the mass of the wings, l is the reference body length, and a is the lateral projected area of the locust.

The wings' contribution to I_{yy} is complex, but may be modelled by representing each wing as a point mass (m_w), giving:

$$\frac{m_w}{\pi}\int_0^{\pi}[x(t)^2 + z(t)^2]dt \qquad (4)$$

for each wing, where π is the period of a half stroke, and where x and z are the instantaneous coordinates of the wing's centre of mass in the body axes. These are closely approximated as:

$$x(t) \approx x_r + r\sin b\cos\gamma(t) \qquad (5)$$

and

$$z(t) \approx z_r + r\cos b\cos\gamma(t)\ , \qquad (6)$$

where r is the distance from the centre of mass of the wing to the wing root, b is the angle of the stroke plane back from the vertical, and γ is the positional angle of the wings, defined as the angle between the long axis of the wing and the z-axis (all angles in radians). Equations 5 and 6 are exact if the centre of mass lies on the long axis of the wing. The centre of mass was determined by balancing the frozen wings on a pin (the hindwings had to be dried first to spread the vannal fan), and was located approximately one third of the way out on both the forewings and the hindwings.

Weis-Fogh (1956a) showed that the wingbeat of tethered locusts approximates simple harmonic motion if upstroke and downstroke are treated separately. Baker (1979) has shown that the wingbeat is even more closely sinusoidal in free flight. We therefore have:

$$\gamma = \tfrac{1}{2}\varphi\sin t + \bar{\gamma} \qquad (7)$$

for each half stroke, where $0 \le t \le \pi$, φ is the total stroke excursion, and $\bar{\gamma}$ is the mean positional angle of the wings. The kinematic parameters of the 'standard' stroke defined by Weis-Fogh (1956a) are given in Table 2 and were used to evaluate the wings' mean contribution to I_{yy}. Equation 5 was evaluated numerically for the fore- and hindwings of each locust in Maple 6 (Maplesoft Waterloo, ON, Canada) on an Apple G4 PowerMac. Compared to gliding flight, flapping approximately doubles the wings' mean contribution to I_{yy}, by increasing the average moment arm about the pitching axis. The mean contribution of the wings was nevertheless small, always averaging less than 3.5% of I_{yy} (Table 3).

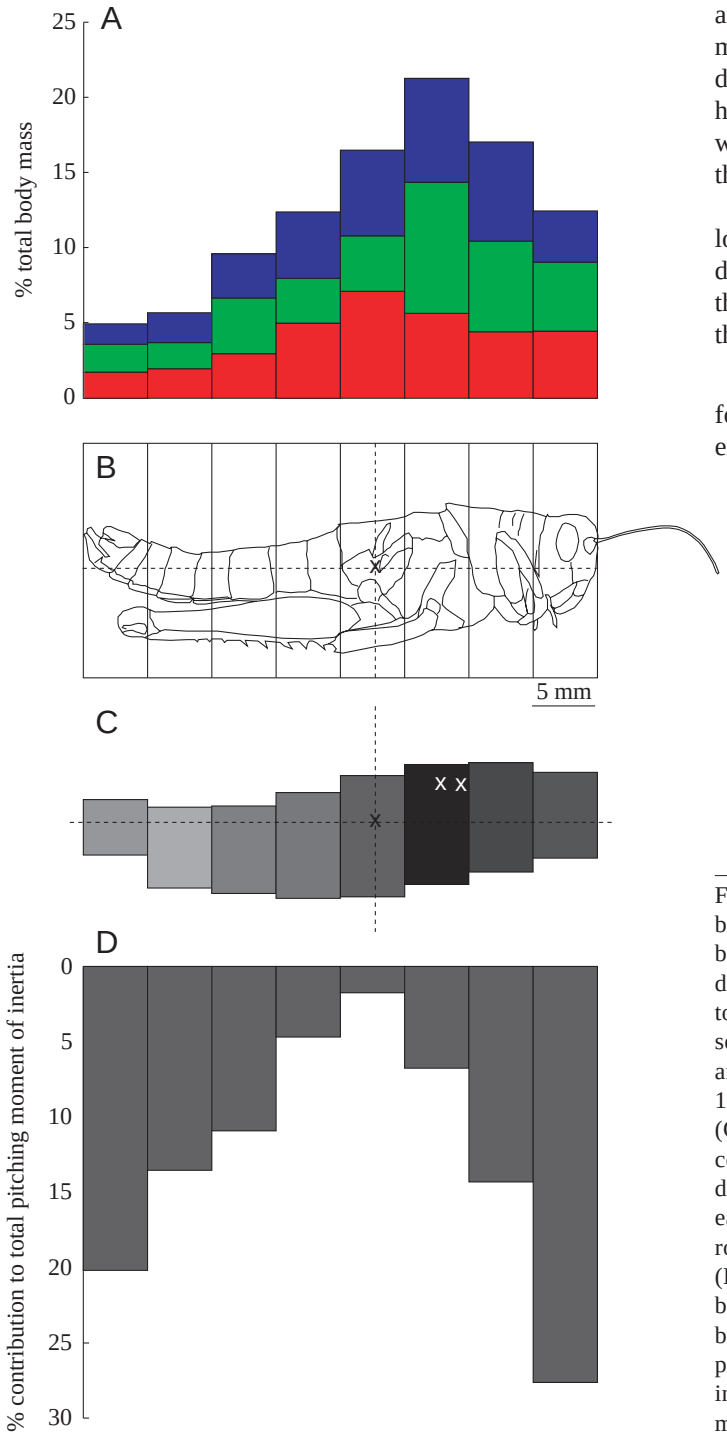

Fig. 5. Pitching moment of inertia (I_{yy}) measurements. (A) Stacked bar graphs showing the masses of eight transverse sections of the body corresponding to the sections illustrated in (B) below. The different colours distinguish data from the three locusts according to the scheme 'R' (red), 'G' (green), 'B' (blue). The mass of each section is expressed as a proportion of the total frozen body mass and the y-axis is scaled such that the total area of the bar graphs is 100%. (B) Line drawing showing the position of the eight sections. (C) Block model of a locust. The area of each of the blocks corresponds to the projected area of each section in B and the density of the shading corresponds to the mass per unit area of each section. The white crosses mark the positions of the wing roots. The red cross marks the position of the centre of mass. (D) Bar graph illustrating the percentage contribution of each body section to the total pitching moment of inertia. Note that this bar graph mirrors the bar graph in A above, indicating that percentage contributions to the total pitching moment of inertia are inversely correlated with percentage contributions to the total body mass.

Table 2. *Kinematic parameters of a 'standard' locust wing stroke*

'Standard' stroke kinematic parameters (degrees)	Forewing	Hindwing
b	33	29
φ	68	110
$\bar{\gamma}$	90	88

'Standard' locust wing stroke as defined by Weis-Fogh (1956a).
b, stroke plane angle; φ, total stroke excursion; $\bar{\gamma}$, mean positional angle of the wings, defined as the mean angle between the long axis of the wing and the *z*-axis.

Results

Analysis of variance for the force measurements

For ease of comparison with the literature, the results of the force measurements are described as relative lift, thrust–drag and pitching moment, before conversion to the form used in the longitudinal system matrix (Equation 2). Figs 6–8 plot the angle series and speed series data, with Model I least-squares linear regressions (see, for example, Sokal and Rohlf, 1995) fitted to the data for each individual (called 'individual regressions'). We combined the data for the three locusts in various General Linear Model (GLM) analyses to test the overall significance of the results for each of the dimensionless forces and moments, including *individual* in the model as a random effect and U or α_b as a covariate (see Table 4 for models used). In all but one case (and then only in the unpaired analysis), relationships that were significant in the individual regressions also attained overall significance in the GLM, affirming that the individual regressions do not lead us to overestimate the significance of the results. *Post hoc* residual analysis indicated that the assumptions of normality of error and homogeneity of variance were fulfilled.

For subsonic fixed-wing aircraft, the aerodynamic forces and moments vary quadratically with flight speed and linearly with angle of attack only up to the stall point. Linear approximations can therefore only be used to model the effects of small changes in speed and pitch, as in the small disturbance formulation of the rigid body equations of motion used here. It is not clear in advance whether we should expect the aerodynamic forces and moments to vary similarly in locusts, which appear to use unsteady aerodynamics (Cloupeau et al., 1979; Wilkin, 1990) and may also vary their wing kinematics with changes in speed and attitude. Nevertheless, for the range of disturbances studied, the forces and moments were all well modelled as linear functions of U and α_b. Although relative thrust–drag and pitching moment both varied significantly with U^2 ($P<0.0001$) when U^2 was treated as the covariate, no significant quadratic term could be found in any hierarchical GLM of the form L_r=*individual*+U+U*U in which U was treated as the covariate. There is therefore no evidence for any significant quadratic effect over and above a linear dependency of the aerodynamic forces and moments on U.

Table 3. *Contributions to the total pitching moment of inertia* I_{yy}

	Contribution to I_{yy} (10^{-9} kg m^2)					
Locust	Total body	Forewing (flapping)	Forewing (gliding)	Hindwing (flapping)	Hindwing (gliding)	Total I_{yy}
'R'	232.8	4.0	2.9	4.1	1.5	240.9
'G'	140.3	2.6	1.8	2.6	0.8	145.4
'B'	236.0	3.4	2.5	3.4	1.3	242.8

Table 4. *Table of* P*-values from the General Linear Model (GLM) analyses*

		P-values		
General Linear Model	Source of data	Covariate	*individual*	Interaction
L_r=*individual*+α_b+α_b**individual*	Unpaired angle series	**<0.001**	0.070	0.064
L_r=*individual*+α_b+α_b**individual*	Paired angle series	**<0.001**	**<0.001**	**<0.001**
L_r=*individual*+U+U**individual*	Speed series	**0.047**	**0.003**	0.373
T_r=*individual*+α_b+α_b**individual*	Unpaired angle series	**0.024**	**<0.001**	0.275
T_r=*individual*+α_b+α_b**individual*	Paired angle series	**<0.001**	**<0.001**	0.058
T_r=*individual*+U+U**individual*	Speed series	**<0.001**	**<0.001**	0.461
M_r=*individual*+α_b+α_b**individual*	Unpaired angle series	0.065	**<0.001**	0.244
M_r=*individual*+α_b+α_b**individual*	Paired angle series	**<0.001**	**<0.001**	**0.025**
M_r=*individual*+U+U**individual*	Speed series	**<0.001**	**<0.001**	0.101

Significant terms ($P<0.05$) in the models are highlighted in bold. The *P*-values for the main effects are calculated using adjusted sums of squares, with only the main effects included in the model.

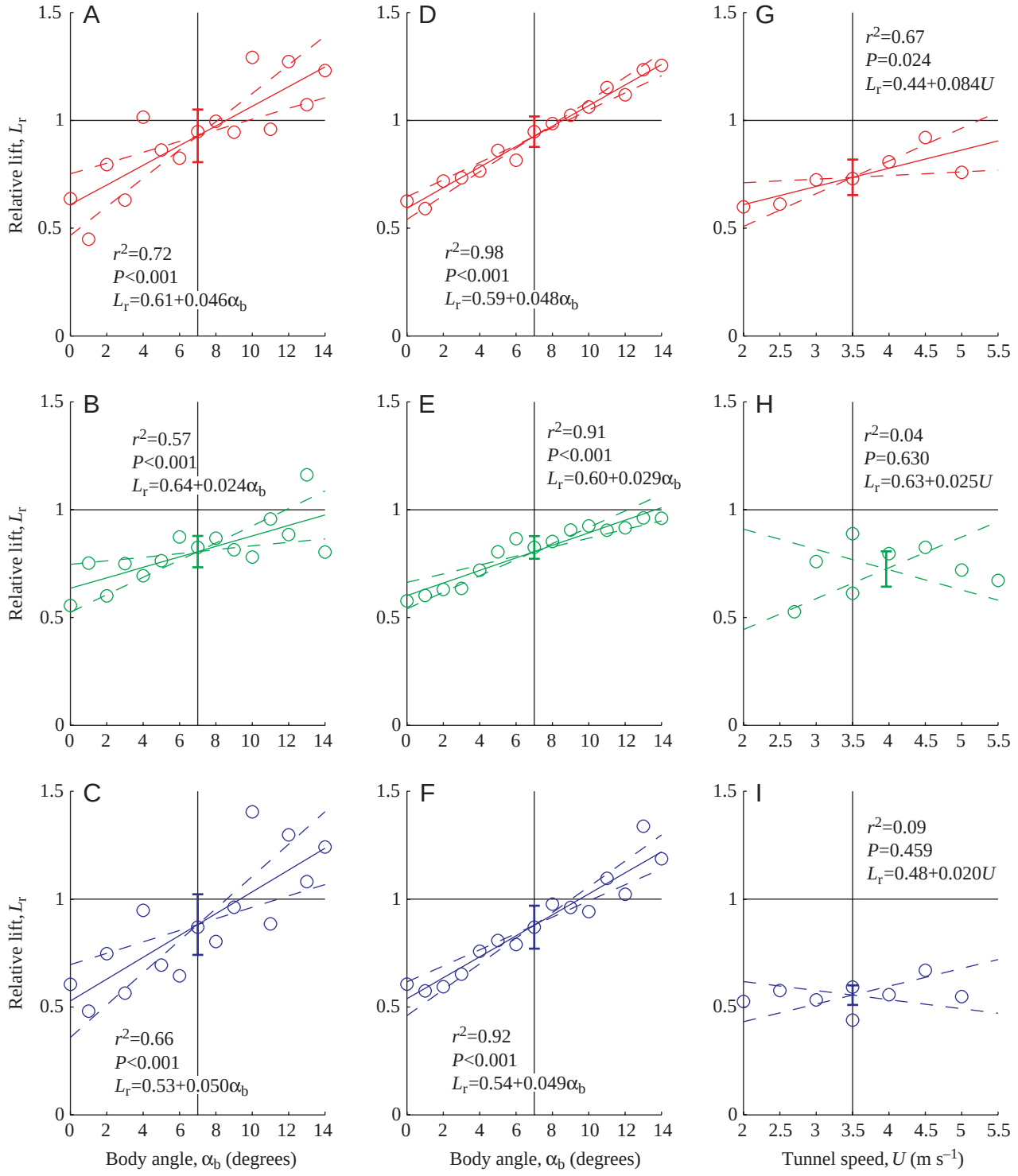

Fig. 6. Graphs of relative lift L_r against α_b for the unpaired (A–C) and paired (D–F) analyses of the angle series data, and against U (G–I) for the speed series data. The usual red/green/blue colour coding of the locusts applies. Horizontal black lines denote equilibrium levels of dimensionless force production. Vertical black lines denote the reference speed U_{ref} and body angle $\alpha_{b,ref}$. In each of A–F, the single data point at 7° represents the mean of the 14 measurements at $\alpha_{b,ref}$. Regression lines are only drawn if the slope of the individual regression was significant and if U or α_b attained overall significance in the corresponding pooled general linear model. The error bars on the regressions for the unpaired analysis (A–C, G–I) show the 95% confidence interval for the regression mean (±1.96 S.E.M.). The error bars on the regressions for the paired analyses (D–F) show the 95% confidence interval for the mean of the 14 reference measurements (±1.96 S.E.M.), which in this case provides the only independent estimate of the height of the curve above the x-axis. The broken lines represent the 95% confidence interval for the slope of the regression plus the 95% confidence interval for the slope of the corrections for tunnel speed or balance orientation. Note that the combined confidence interval for the slope may include zero even if the P-value for the regression slope itself is significant.

The term *individual* was significant in all but one of the GLM analyses (Table 4), because locust 'G' produced significantly less force in proportion to its body mass than either of the other locusts. The interaction term *individual**α_b was significant for the GLM of the paired data for L_r (P<0.001) and M_r (P=0.025), and only just non-significant for the paired data for T_r (P=0.058), indicating that the slopes of the dimensionless forces and moments against α_b do differ significantly between individuals. The interaction *individual**α_b was not significant in any of the unpaired

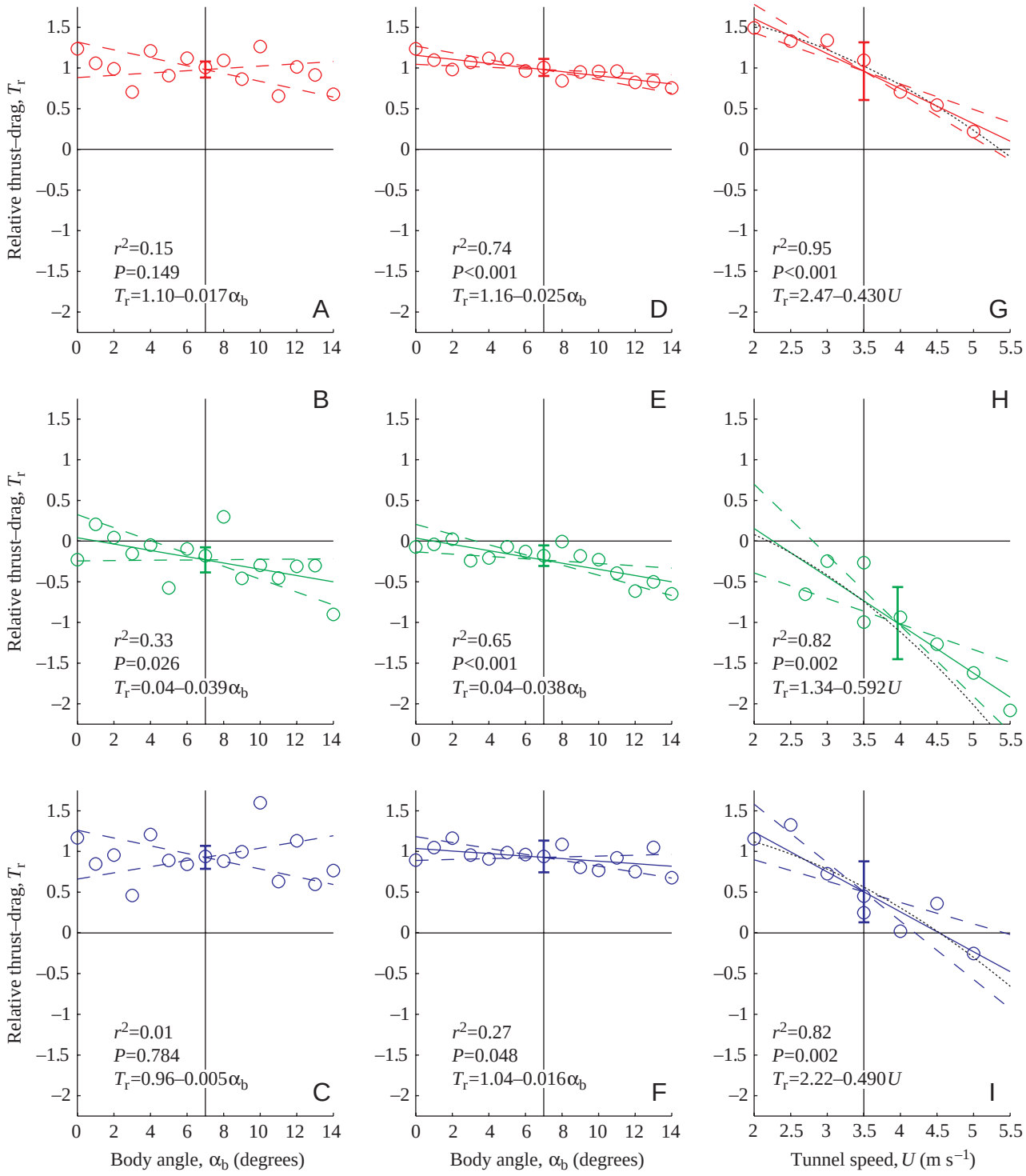

Fig. 7. Graphs of relative thrust–drag T_r against α_b for the unpaired (A–C) and paired (D–F) analyses of the angle series data, and against U (G–I) for the speed series data. For further explanation, see legend to Fig. 6. Individual regressions of T_r against U^2 (G–I) are shown as black dotted lines where the individual regression and the corresponding GLM treating U^2 as the covariate were both significant; it is clear that the deviation from linearity is small over the range of speeds used.

analyses, suggesting that the paired analyses are more sensitive and better at picking up subtle differences between individuals. On average, the paired analyses explain 33% more of the total variation than the unpaired analyses, as can be seen from the dramatic decrease in scatter between the graphs of the unpaired and paired analyses (Figs 6–8).

The tighter fit of the data from the paired analysis is a good indication that the locusts' flight performance varied through

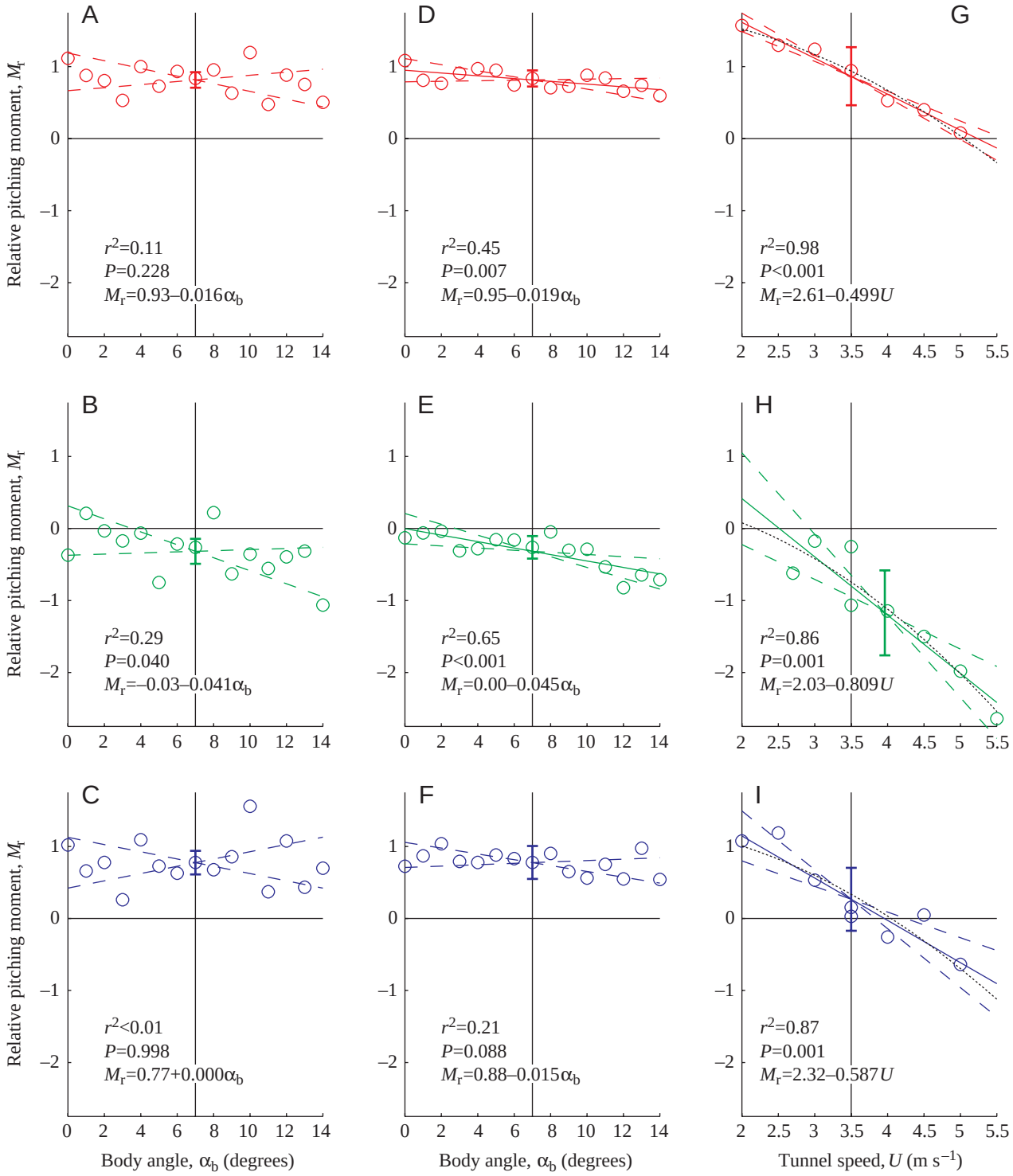

Fig. 8. Graphs of relative pitching moment M_r against α_b for the unpaired (A–C) and paired (D–F) analyses of the angle series data, and against U (G–I) for the speed series data. For further explanation, see legend to Fig. 6. Individual regressions of M_r against U^2 (G–I) are shown as black dotted lines where the individual regression and the corresponding GLM treating U^2 as the covariate were both significant; it is clear that the deviation from linearity is small over the range of speeds used.

time. This is shown directly in Fig. 9, which plots L_r against time for the angle series; equivalent graphs for T_r and M_r are of similar form. Locusts 'R' and 'B' produced decreasing amounts of lift over time, but, surprisingly, locust 'G' actually increased the lift it produced. In all three cases, temporal lift variation (indicated by the range of the reference measurements) is of the same order of magnitude as pitch-dependent lift variation (indicated by the range of scatter about the line joining the reference measurements in Fig. 9): temporal variation in aerodynamic force production cannot be ignored (*contra* Weis-Fogh, 1956a,b). Mismatches between the reference levels of force production measured in the consecutive angle and speed series experiments are presumably the result of temporal variation in flight performance.

Relative lift

All three locusts produced lift in excess of body weight at certain times during the angle series but below body weight at others (Fig. 6A–C), so each must have supported their body weight exactly at some point in time. The mean lift generated by locusts 'R' and 'B' was not significantly different from body weight over the angle series as a whole. None of the locusts ever produced lift in excess of body weight during the speed series (Fig. 6G–I), but this is not surprising in light of the general decline in lift production through time observed in locusts 'R' and 'B' (Fig. 9). The decline in L_r might also indicate some form of physiological compensation for the loss of body mass, although the percentage changes in body mass are relatively small (<6%).

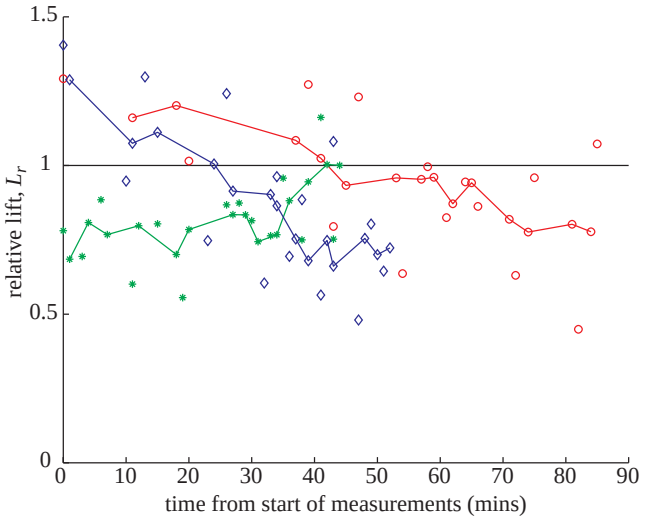

Fig. 9. Graph of relative lift L_r against time through the angle series experiments. The usual red/green/blue colour coding of the locusts applies. The horizontal black line denotes the equilibrium level of relative lift production. Coloured lines join the 14 reference measurements at $\alpha_{b,ref}$. The vertical range of the lines gives an indication of how lift production varies through time. The range of scatter about the lines gives an indication of the relative magnitude of variation in lift due to changes in α_b.

Relative lift increased linearly with α_b over the range of disturbances studied (Fig. 6A–F). This increase was highly significant ($P<0.001$) in the GLM analyses using both the paired and unpaired methods (Table 4), and was just as highly significant in the individual regressions (Fig. 6A–F). Importantly, the upper and lower confidence limits for the slopes of the lines of L_r against α_b remain positive even when the confidence interval for the correction for balance orientation is added to the confidence interval for the regression slope (Fig. 6A–F; see figure legend). Errors in correcting for balance orientation are therefore small enough not to affect any of the qualitative conclusions above, and we can be confident that the positive relationship between L_r and α_b is both real and consistent across the three individuals. In addition, the r^2 values of the individual regressions were very high, with α_b explaining 91–98% of the within-individual variation in L_r for the paired analysis (Fig. 6D–F). The GLM L_r=*individual*+α_b explained a similar proportion of the total variation in the paired analysis (R^2=0.91), and explained only slightly less of the total variation than the equivalent GLM including the highly significant ($P<0.001$; Table 4) interaction term *individual**α_b (R^2=0.94). This implies that such individual differences in the underlying slopes as may exist are small in the context of the overall variation in L_r. In the GLM analyses, α_b explains 84% of the total variation, based on the sequential sums of squares.

Relative lift increased just significantly (P=0.047) with U in the GLM L_r=*individual*+U (Table 4), but inspection of the individual regressions (Fig. 6G–I) shows that only locust 'R' shows any significant effect. Neither locust 'G' nor locust 'B' offered any evidence of L_r varying linearly with U, but the data are too widely scattered to discount the possibility that some form of relationship exists. The same was true for individual regressions of L_r against U^2, which only showed a significant effect of U^2 for locust 'R' (P=0.039), and even then the corresponding GLM treating U^2 as a covariate failed to attain overall significance.

Relative thrust–drag

Locust 'R' always produced a net thrust, as did locust 'B' except at the highest tunnel speed (Fig. 7). Only locust 'G' alternated between producing net thrust and net drag (Fig. 7). The preferred flight speeds of locusts 'R' and 'B' are therefore likely to be higher than for locust 'G', consistent with their larger overall size (some 30% greater by body mass).

Relative thrust–drag decreased linearly with α_b over the range of disturbances studied (Fig. 7D–F). The negative slope of the GLM T_r=*individual*+α_b was just significant (P=0.024) for the unpaired analysis (Table 4), but since only the individual regression for locust 'G' showed any significant effect (P=0.026), the unpaired analysis offers no strong evidence for a general effect of body angle on thrust–drag (Fig. 7A–C). On the other hand, the GLM T_r=*individual*+α_b revealed a highly significant ($P<0.001$) negative relationship between T_r and α_b in the paired analysis (Table 4), and in this case the negative slopes of the individual regressions were

highly significant (P<0.001) for locusts ‘R’ and ‘G’ (Fig. 7D,E) and just significant (P=0.048) for locust ‘B’ (Fig. 7F). In the case of locust ‘B’, the confidence interval widened just enough to include zero when error in correcting for balance orientation was taken into account (Fig. 7F). Nevertheless, the negative relationship between T_r and α_b that was weakly detected by the unpaired analysis is clearly revealed by the more sensitive paired analysis, and we can be reasonably confident that this relationship is both real and consistent across the three individuals. Although the GLM T_r=*individual*+α_b explained an extremely high proportion of the total variation in the paired analysis (R^2=0.96), this largely reflects the wide variation in T_r between individuals, which tends to swamp the variation due to α_b in the pooled analysis. In fact, the term *individual* explains over 92% of the total variation in the GLM, whereas α_b explains only 4%. Under these circumstances, the r^2 values for the individual regressions (average r^2=0.55) give a better indication of the importance of α_b in explaining variation in T_r – at least within individuals.

A highly significant negative relationship was found between T_r and U (P<0.001) in the GLM T_r=*individual*+U (Table 4). The significance levels of the individual regressions (Fig. 7G–I) were also very high (P≤0.002), and all showed a negative relationship between T_r and U. We are therefore confident that this relationship is both real and consistent across individuals, which is reassuring because a negative relationship between T_r and U is necessary to provide static stability with respect to flight speed. Individual regressions of T_r against U^2 were also highly significant (P≤0.004), as was the corresponding GLM treating U^2 as the covariate (P<0.001), so the individual regressions of T_r against U^2 are plotted for comparison with the linearized response to small perturbations (Fig. 7G–I): it is clear that the deviation from linearity is small over the range of speeds used. Although the total proportion of the variation explained by the GLM T_r=*individual*+U was very high (R^2=0.95), U explained only 23% of the total variation in T_r when fitted after *individual* in the model (note that for the speed series analysis, the sequential and adjusted sums of squares generally differ). Once again, the r^2 values of the individual regressions (average r^2=0.91) give a better indication of the importance of U in explaining variation in T_r.

Relative pitching moment

Locust ‘R’ consistently produced a nose-up pitching moment (Fig. 8), and is therefore unlikely to have experienced pitch equilibrium at any point in the experiments. Locusts ‘G’ and ‘B’ both produced nose-up and nose-down pitching moments at various moments in time (Fig. 8), so both must have experienced pitch equilibrium at some point.

The GLM M_r=*individual*+α_b for the unpaired analysis was the only GLM in which the slope was not quite significant (P=0.065), but the more sensitive paired analysis was able to resolve the underlying relationship, with a highly significant (P<0.001) negative relationship found in the corresponding GLM (Table 4). A negative relationship between M_r and α_b was found in all of the individual regressions (Fig. 8A–F), although the slope for locust ‘B’ just failed to attain significance (P=0.088). The slopes for locusts ‘R’ and ‘G’ were both highly significant (P=0.007, P<0.001, respectively), although the confidence interval for locust ‘R’ widened just enough to include zero when error in correcting for balance orientation was taking into account (Fig. 8D). Nevertheless, the consistency with which a negative slope was found gives us confidence in the generality of the relationship, which is reassuring because a negative relationship between M_r and α_b is essential for static pitch stability. The GLM M_r=*individual*+α_b explained a very high proportion of the total variation in the paired analysis (R^2=0.94), but as in the analysis of thrust–drag, α_b itself explained a relatively small proportion (4%) of this variation, owing to the much smaller relative force production of locust ‘G’ as compared to locusts ‘R’ and ‘B’. Here again, the r^2 values of the individual regressions give a better indication of the proportion of the variation in M_r explained by α_b (average r^2=0.44). As in the analysis of lift, the proportion of the variation in M_r explained by the GLM M_r=*individual*+α_b was only 1% less than the proportion explained by the corresponding GLM including the significant interaction (P=0.025) term. Such individual differences in the underlying slopes as may exist are therefore likely to be small in the context of the overall variation in M_r.

All of the individual regressions of M_r against U (Fig. 8G–I) had a highly significant (P≤0.001) negative slope, and explained a high proportion of the within-individual variation in M_r (r^2=0.90 on average). This was mirrored by the high significance (P<0.001) of the GLM M_r=*individual*+U (Table 4) and the very high proportion of the total variation explained by the model (R^2=0.94), although U itself explained only 31% of the total variation in M_r when fitted after *individual* in the model. Incorporating the 95% confidence interval for the correction for U did not widen the combined confidence intervals for the slopes of the individual regressions to include zero (Fig. 8G–I), and we are therefore confident that this negative relationship between M_r and U is both real and consistent across the three individuals. Individual regressions of M_r against U^2 were also highly significant (P≤0.002), as was the corresponding GLM treating U^2 as the covariate (P<0.001), so the individual regressions of M_r against U^2 are plotted for comparison with the linearized response to small perturbations (Fig. 8G–I): it is clear that the deviation from linearity is small over the range of speeds used.

Analysis of results

Populating the system matrix

The fact that L_r, T_r and M_r are so well modelled as linear functions of small perturbations to α_b and U substantially validates the linearization of the equations within the range of disturbances studied, and also suggests that the slopes of the regressions will give a good estimate of the slopes of the underlying relationships at equilibrium. Because α_b was held constant whilst U was varied, and *vice versa*, the slopes of

these functions already define partial derivatives like those in the longitudinal system matrix $\mathbf{F}_{sym}$ (Equation 2), with the important caveat that because flight equilibrium was never achieved for the combinations of α_b and U we used, we must assume that the same slopes would apply for small disturbances from equilibrium. This assumption allows us to calculate all of the stability derivatives in Equation 2, except for the pitch rate derivatives (q-derivatives), and conveniently preserves the linear time-invariance of the equations. Our general strategy will be to analyse the system matrix assuming that the pitch rate derivatives are all zero, and then to investigate the effect of assigning a range of realistic non-zero values to them. This means that the empirically-defined longitudinal system matrices contain only the static stability derivatives (i.e. X_u, Z_u, M_u, X_w, Z_w, M_w), and we will term them 'static system matrices' to highlight this important qualification.

Whereas we have so far presented force data resolved into vertical lift and horizontal thrust–drag components, the stability derivatives in $\mathbf{F}_{sym}$ are resolved into X and Z components fixed with respect to the body. The corresponding axes are usually defined such that the x-axis is aligned with the direction of flight at equilibrium, which means that $w_e=\theta_e=0$. The axes are then referred to as stability axes. With these simplifications, we may write the equation of motion for non-manoeuvring flight with correctional control enabled as:

$$\begin{bmatrix} \delta\dot{u} \\ \delta\dot{w} \\ \delta\dot{q} \\ \delta\dot{\theta} \end{bmatrix} = \begin{bmatrix} \frac{X_u}{m} & \frac{X_w}{m} & 0 & -g \\ \frac{Z_u}{m} & \frac{Z_w}{m} & u_e & 0 \\ \frac{M_u}{I_{yy}} & \frac{M_w}{I_{yy}} & 0 & 0 \\ 0 & 0 & 1 & 0 \end{bmatrix} \begin{bmatrix} \delta u \\ \delta w \\ \delta q \\ \delta\theta \end{bmatrix}, \quad (8)$$

where the 4×4 matrix is the static system matrix. Equation 8 explicitly requires that we specify the equilibrium flight speed (u_e) and implicitly requires that we specify the equilibrium body angle ($\alpha_{b,e}$) in order to define the axes in which the forces are to be resolved. Unfortunately, it is not possible to determine whether a locust was flying at equilibrium in advance of analysing the flight data. Not surprisingly, none of the locusts ever flew in perfect equilibrium (i.e. lift balancing body weight, thrust balancing drag, and no net pitching moment), but the reference measurements taken during the angle series experiments provide reliable benchmarks from which to solve for the equilibrium flight condition, about which the equations of motion are linearized.

Since the individual locusts differed significantly in their flight performance, we will calculate the equilibrium flight conditions and stability derivatives separately for each individual. In general, we have:

$$L_r = L_{r,ref} + \frac{\partial L_r}{\partial \alpha_b}(\alpha_b - \alpha_{b,ref}) + \frac{\partial L_r}{\partial U}(U - U_{ref}) \quad (9a)$$

$$T_r = T_{r,ref} + \frac{\partial T_r}{\partial \alpha_b}(\alpha_b - \alpha_{b,ref}) + \frac{\partial T_r}{\partial U}(U - U_{ref}) \quad (9b)$$

$$M_r = M_{r,ref} + \frac{\partial M_r}{\partial \alpha_b}(\alpha_b - \alpha_{b,ref}) + \frac{\partial M_r}{\partial U}(U - U_{ref}), \quad (9c)$$

where $L_{r,ref}$, $T_{r,ref}$ and $M_{r,ref}$ denote the mean levels of relative force production at the reference speed (U_{ref}=3.50 m s^{-1}) and body angle ($\alpha_{b,ref}$=7°). Solving for the equilibrium flight conditions means solving Equation 9a–c for L_r=1 and T_r=M_r=0. Unfortunately, since we have three dependent variables (lift, thrust–drag and pitching moment), but only two independent variables (speed and body angle), it is only possible to solve the equations such that two of the three equilibrium conditions are satisfied. Pitch disequilibrium and thrust–drag disequilibrium are closely linked in our dataset, so we will solve Equation 9a–c for L_r=1, letting either T_r=0 or M_r=0. This gives two pseudo-equilibria, which each provide an estimate of the equilibrium tunnel speed (U_e), and may be averaged to give the unique estimate of u_e that we require (in practice the two estimates always differed by less than 13% of their mean). The solution for $\alpha_{b,e}$ is already unique if we assume, as shown above, that lift is independent of flight speed (i.e. $\partial L_r/\partial U$=0). The pseudo-equilibria so defined (Table 5) are consistent with the speeds and body angles adopted by free-flying locusts in the wild (*Schistocerca gregaria*: Waloff, 1972; *Locusta migratoria*: Baker et al., 1981).

Having defined $\alpha_{b,e}$ for each of the locusts, we may resolve the forces into X and Z components. Calculating the stability derivatives directly from the regressions of L_r and T_r against

Table 5. *Measurements of mean relative lift* $L_{r,ref}$*, mean relative thrust–drag* $T_{r,ref}$ *and mean relative pitching moment* $M_{r,ref}$ *at the reference flight condition (*U_{ref}*=3.50 m s*$^{-1}$*;* $\alpha_{b,ref}$*=7°), together with their partial derivatives with respect to tunnel speed* U *and body angle* α_b*, and the calculated pseudo-equilibria for tunnel speed* U_e *and body angle* $\alpha_{b,e}$

	Measured parameters									Pseudo-equilibrium solutions		
											U_e (m s^{-1})	
Locust	$L_{r,ref}$	$T_{r,ref}$	$M_{r,ref}$	$\partial L_r/\partial\alpha_b$ (deg s^{-1})	$\partial T_r/\partial\alpha_b$ (deg s^{-1})	$\partial M_r/\partial\alpha_b$ (deg s^{-1})	$\partial L_r/\partial U$ (m^{-1} s)	$\partial T_r/\partial U$ (m^{-1} s)	$\partial M_r/\partial U$ (m^{-1} s)	$\alpha_{b,e}$ (degrees)	T_r=0	M_r=0
'R'	0.95	1.01	0.84	0.048	–0.025	–0.019	*	–0.43	–0.50	8	5.78	5.13
'G'	0.83	–0.18	–0.26	0.029	–0.038	–0.045	*	–0.59	–0.81	13	2.81	2.84
'B'	0.87	0.94	0.78	0.049	–0.016	–0.015	*	–0.49	–0.59	10	5.33	4.75

Table 6. *Dimensional static stability derivatives with respect to tunnel speed* U *and body angle* α_b *for the three locusts, resolved in the stability axes*

Locust	$\partial X/\partial\alpha_b$ (10^{-3} N rad^{-1})	$\partial Z/\partial\alpha_b$ (10^{-3} N rad^{-1})	$\partial M/\partial\alpha_b$ (10^{-6} N m rad^{-1})	$\partial X/\partial U$ (10^{-3} N m^{-1} s)	$\partial Z/\partial U$ (10^{-3} N m^{-1} s)	$\partial M/\partial U$ (10^{-6} N s)
'R'	–9.9	–31	–924	–7.8	–1.4	–416
'G'	–23	–25	–1467	–8.3	[0.53]	–461
'B'	[–1.5]	–34	[–739]	–9.0	[0.05]	–492

α_b and U complicates interpretation of the regression model used, so we instead resolved the forces into their X and Z components and fitted Model I linear regressions to the data again. The slopes of these regressions are given as partial derivatives in Table 6 and are shown enclosed in square brackets if the individual regression slope was non-significant ($P>0.05$). It is immediately clear that the stability derivatives are more reliable for locusts 'R' and 'G' than for locust 'B'. The significance of the regressions closely matches that of the regressions of L_r and T_r; for example, the non-significant Z_u derivatives for locusts 'G' and 'B' in Table 6 reflect the absence of any significant relationship between L_r and U for those individuals.

The partial derivatives of Table 6 must now be re-expressed as functions of the longitudinal velocity components u and w in order to match the form of the stability derivatives in Equation 8. For the symmetrical flight condition, we have:

$$U = \sqrt{u^2 + w^2} \tag{10}$$

and since w^2 is well over an order of magnitude smaller than u^2, even at the most extreme body angles used in the experiments, the first order approximation

$$U \approx u = u_e + \delta u \tag{11}$$

is perfectly acceptable at perturbed angles of attack. The u-derivatives may therefore be expressed as:

$$X_u = \frac{\partial X}{\partial u} \approx \frac{\partial X}{\partial U}, \quad Z_u = \frac{\partial Z}{\partial u} \approx \frac{\partial Z}{\partial U}, \quad M_u = \frac{\partial M}{\partial u} \approx \frac{\partial M}{\partial U}. \tag{12}$$

Similarly, we may express α_b as:

$$\alpha_b = \alpha_{b,e} + \tan^{-1}(w/u) = \alpha_{b,e} + \tan^{-1}[\delta w/(u_e+\delta u)], \tag{13}$$

which indicates that to a first-order approximation,

$$\partial w \approx u_e \partial\alpha_b, \tag{14}$$

where α_b is in radians. Hence, the w-derivatives are simply:

$$X_w = \frac{\partial X}{\partial w} \approx u_e^{-1}\frac{\partial X}{\partial\alpha_b}, \quad Z_w = \frac{\partial Z}{\partial w} \approx u_e^{-1}\frac{\partial Z}{\partial\alpha_b},$$
$$M_w = \frac{\partial M}{\partial w} \approx u_e^{-1}\frac{\partial M}{\partial\alpha_b} \tag{15}$$

allowing us to calculate all six static stability derivatives for each locust (Table 7), and so to populate the system matrix in Equation 8.

Solution of the small disturbance equations

To yield any useful insight into locust flight we must use the system matrices we have defined to solve Equation 8, which is of the general form:

$$\dot{\mathbf{x}}(t) = \mathbf{A}\mathbf{x}(t). \tag{16}$$

Solutions to this first-order differential equation are well known and are of the general form:

$$\mathbf{x}(t) = e^{t\mathbf{A}}\mathbf{x}(0), \tag{17}$$

where $e^{\mathbf{A}}$ is the matrix exponential (e.g. Apostol, 1997). This is shown by differentiating Equation 17 with respect to t:

$$\dot{\mathbf{x}}(t) = \mathbf{A}e^{t\mathbf{A}}\mathbf{x}(0) = \mathbf{A}\mathbf{x}(t). \tag{18}$$

The exponential matrix $e^{t\mathbf{A}}$ is readily calculated if the $n\times n$ matrix $\mathbf{A}$ can be diagonalized (which is the case if its n eigenvalues are distinct), in which case we have:

$$e^{t\mathbf{A}} = \mathbf{C}e^{t\mathbf{D}}\mathbf{C}^{-1}, \tag{19}$$

where $\mathbf{C}$ is a non-singular matrix depending on $\mathbf{A}$, and $\mathbf{D}$ is an $n\times n$ diagonal matrix with the same eigenvalues ($\lambda_1,\ldots,\lambda_n$) as $\mathbf{A}$. Hence,

$$\mathbf{x}(t) = \mathbf{C}e^{t\mathbf{D}}\mathbf{C}^{-1}\mathbf{x}(0), \tag{20}$$

and since

$$e^{t\mathbf{D}} = \mathrm{diag}(e^{t\lambda_1},\ldots,e^{t\lambda_n}), \tag{21}$$

Table 7. *Dimensional static stability derivatives with respect to forward speed (*u*) and aerodynamic incidence (*w*) for the three locusts, resolved in the stability axes*

Locust	u_e (m s^{-1})	X_u (10^{-3} N m^{-1} s)	Z_u (10^{-3} N m^{-1} s)	M_u (10^{-6} N s)	X_w (10^{-3} N m^{-1} s)	Z_w (10^{-3} N m^{-1} s)	M_w (10^{-6} N s)
'R'	5.45	–7.8	–1.4	–416	–1.8	–58	–170
'G'	2.82	–8.3	0.53	–461	–8.0	–9.0	–520
'B'	5.04	–9.0	0.050	–492	–0.31	–6.7	–147

The estimated equilibrium flight speed (u_e) is also given.

Table 8. *Roots, or eigenvalues, of the characteristic equation for each of the three locusts*

Locust	Roots of characteristic equation		
	$\lambda_{1,2}$	λ_3	λ_4
'R'	–4.9±62*i*	5.0	–2.5
'G'	–7.1±100*i*	5.7	–3.5
'B'	–5.3±55*i*	6.0	–3.9

Note that each locust has one pair of complex conjugate roots ($\lambda_{1,2}$) with negative real parts (describing a stable oscillatory mode), one positive real root (λ_3, describing an unstable divergence mode), and one negative real root (λ_4, describing a stable subsidence mode).

The real parts of the roots define the damping of the modes.

Imaginary parts define the angular frequency of an oscillatory mode.

it follows that the entries of the exponential matrix $e^{t\mathbf{A}}$ are linear combinations of $e^{t\lambda_1},\ldots,e^{t\lambda_n}$, and therefore (Equation 17) the values of the state variables themselves are also linear combinations of these modes. Table 8 gives the eigenvalues of the static system matrices for each of the locusts, calculated in Matlab.

A positive real root will result in the exponential growth of each of the disturbance quantities in Equations 22, so the modes of motion identified by the positive real roots in Table 8 are dynamically unstable. On the other hand, the negative real roots in Table 8 will result in exponential decay of the disturbed quantities, so the modes of motion that they identify are dynamically stable. The behaviour of a pair of complex conjugate roots $\lambda=n\pm i\omega$ is less straightforward, but since the principle of linear superposition applies, the pair combines to give:

$$\delta u = a_{1,1}e^{(n+i\omega)t} + a_{1,2}e^{(n-i\omega)t},$$
$$\delta w = a_{2,1}e^{(n+i\omega)t} + a_{2,2}e^{(n-i\omega)t}, \text{ etc.}, \quad (22)$$

which can be expanded as:

$$\delta u = e^{nt}(A_{1,1}\cos\omega t + A_{1,2}\sin\omega t),$$
$$\delta w = e^{nt}(A_{2,1}\cos\omega t + A_{2,2}\sin\omega t), \text{ etc.}, \quad (23)$$

where the coefficients $A_{1,1}=(a_{1,1}+a_{1,2})$ and $A_{1,2}=i(a_{1,1}-a_{1,2})$, etc. are real numbers. Equation 23 describes an oscillatory motion of angular frequency ω and period $T=2\pi/\omega$, so the complex conjugate roots identify an oscillatory mode of motion. It is clear by inspection of Equation 23 that this motion decays if the real part, n, of the root is negative, but grows if n is positive. The complex roots in Table 8 always have negative real parts, so the mode of motion that they identify is dynamically stable. The behaviours of the four types of general solution to Equation 16 are indicated in Fig. 10A–D. The three modes of motion displayed by the locusts correspond to the types of general solution illustrated in Fig. 10AC. On the principle of linear superposition, and in the absence of any control inputs beyond those identified in the static system matrices, the natural flight behaviour of a locust is describable as the sum of these three modes. Since one of these modes is unstable, the model fails to explain the dynamic flight stability of locusts completely. We will now consider each of the modes we have identified in detail.

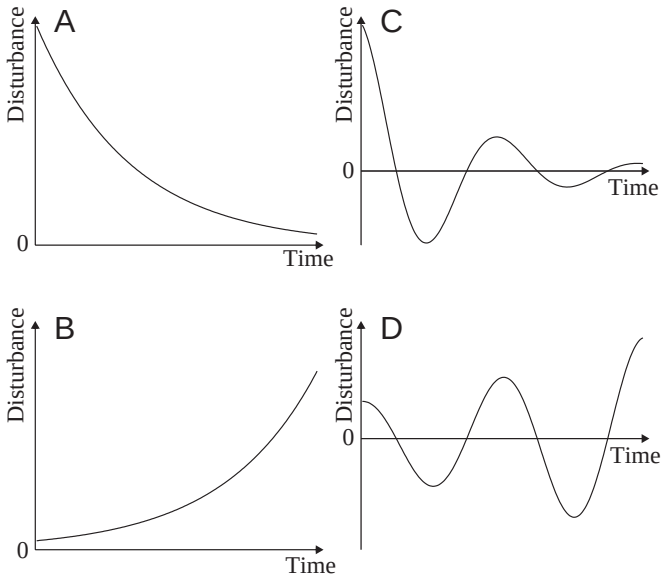

Fig. 10. The four general types of solution to the longitudinal equations of motion. (A) Monotonic subsidence (stable), corresponding to a negative real root. (B) Monotonic divergence (unstable), corresponding to a positive real root. (C) Damped oscillation (stable), corresponding to a complex conjugate pair of roots with negative real parts. (D) Divergent oscillation (unstable), corresponding to a complex conjugate pair of roots with positive real parts.

The damped oscillatory mode

The pair of complex conjugate roots $\lambda=n\pm i\omega$ identify a damped oscillatory mode of relatively short period (T_R=0.10 s, T_G=0.06 s, T_B=0.11 s). The damping of the motion is defined by the damping ratio:

$$\zeta = -n/(\omega^2 + n^2)^{1/2}, \quad (24)$$

which for the three locusts is: ζ_R=0.079, ζ_G=0.071, ζ_B=0.095. Critical damping (i.e. the transition from sinusoidal to exponential motion) occurs at ζ=1, so it is clear that the oscillatory mode is rather lightly damped. This conclusion must be treated with some caution at this stage, because the *q*-derivatives, which were dropped in Equation 8, are an important source of pitch damping in aircraft (Nelson, 1989; Etkin and Reid, 1996; Cook, 1997). Strictly speaking we can only say that the static stability derivatives imply the existence of a lightly damped oscillatory mode of motion. We can quantify the static damping of the motion further by calculating the time taken for an oscillation to halve in magnitude, where:

$$t_{half} = \frac{\ln 2}{|n|}. \quad (25)$$

This yields times to halve that are approximately the same as a single period of oscillation ($t_{half,R}$=0.14 s, $t_{half,G}$=0.10 s, $t_{half,B}$=0.13 s).

Table 9. *Eigenvectors of the characteristic equation for each of the three locusts*

		Eigenvectors							
Locust	Mode	$\delta u/u_e$	Phase angle (degrees)	$\delta w/u_e \approx \delta\alpha_b$	Phase angle (degrees)	δq (rad s^{-1})	Phase angle (degrees)	$\delta\theta$ (rad)	Phase angle (degrees)
'R'	Oscillatory	0.044	–90.4	1.0	–2.9	62	–94.5	1	0
	Divergence	–0.26		0.64		5.0		1	
	Subsidence	2.8		–7.0		–2.5		1	
'G'	Oscillatory	0.090	91.4	1.0	3.6	101	94.1	1	0
	Divergence	–0.52		0.46		5.7		1	
	Subsidence	1.3		–1.1		–3.5		1	
'B'	Oscillatory	0.038	89.8	1.0	3.7	56	95.4	1	0
	Divergence	–0.19		0.62		6.0		1	
	Subsidence	–4.9		16.6		–3.9		1	

Each row of eigenvectors corresponds to one of the roots, or eigenvalues, in Table 7 and gives the relative magnitudes and phases of the state variables that satisfy the corresponding solution to the characteristic equation.

The values of the eigenvectors are arbitrary to within a complex factor, and the eigenvectors are therefore normalised to give the pitch attitude disturbance $\delta\theta$ a magnitude of 1 rad and phase angle of zero.

Further information on the oscillatory mode may be gathered directly from the relevant eigenvectors, which are simply values of $\mathbf{x}(0)$ satisfying Equation 17 for each of the roots in Table 8. The components of the eigenvectors are displayed in Table 9, in polar form: since eigenvectors are unique in direction but not in magnitude we have scaled them to make $\delta\theta=1$. Note that a pitch perturbation of 1 rad (approximately 57°) would be substantial indeed, so the scale is chosen only for convenience. Scaling the eigenvectors in this way aids in comparison of the three locusts, but since the values of the various state variables of a single locust are only significant relative to each other, some further normalisation of the variables is required for ease of comparison. We have already shown that $\partial w \approx u_e \partial\alpha_b$ (Equation 14), so normalising δw by u_e as we have done in Table 9 converts δw to radian measure (i.e. the same units as $\delta\theta$). Normalising δu by u_e similarly brings δu into line with the dimensionless form of δw. We can see immediately from Table 9 that changes in the forward velocity component (δu) are negligible in the oscillatory mode. As a result, oscillatory changes in pitch ($\delta\theta$) manifest themselves as oscillations in angle of attack ($\delta\alpha_b$) of almost identical phase and amplitude to the pitch oscillations themselves. This combination of characters seems to identify this oscillatory mode of locusts with the short period pitching mode of aircraft, which is essentially a rapid pitch oscillation with negligible change in forward velocity (e.g. Nelson, 1989; Etkin and Reid, 1996; Cook, 1997).

The subsidence and divergence modes

The non-oscillatory nature of the subsidence and divergence modes is at first sight puzzling. In most aircraft, the longitudinal equations of motion have two pairs of complex conjugate roots, which means that most aircraft display two oscillatory modes of motion: the short period pitching motion just mentioned, and a second, lightly damped motion of much longer period called the phugoid. The latter is classically described as an interchange between kinetic and potential energy, manifested as a steady rise and fall in altitude (Lanchester, 1908). This is accompanied by slow changes in pitch, which result in the angle of attack remaining substantially constant throughout the motion. Assuming it is correct to identify the oscillatory mode found in locusts with the short period mode of aircraft, then the results of this analysis show the complex phugoid root of aircraft appears to split into two real roots in locusts.

The lack of any clear relationship between lift and flight speed in our results (see also Zarnack and Wortmann, 1989) goes a long way towards explaining this difference. The apparent independence of speed and lift is most clearly manifested in the speed derivative Z_u, which is statistically non-significant ($P>0.05$) in locusts 'G' and 'B'. This speed derivative plays a critical role in the phugoid motion of aircraft, because potential energy lost as the aircraft loses altitude is converted into kinetic energy with a concomitant increase in speed. This increase in speed increases the lift and causes the aircraft to gain altitude, so it is the speed derivative Z_u that is responsible for the oscillatory behaviour of the phugoid. Given the lack of any clear relationship between lift and flight speed in locusts, it is not surprising to find that they exhibit no analogous oscillatory mode.

Although the two real roots identify modes that are non-oscillatory, it is nevertheless possible to gain some impression of the timescales on which they operate by specifying the time to halve or double (Equation 25). This gives: $t_{half,R}=0.28$ s, $t_{half,G}=0.20$ s, $t_{half,B}=0.18$ s, for the subsidence mode, and $t_{double,R}=0.14$ s, $t_{double,G}=0.12$ s, $t_{double,B}=0.12$ s for the divergence mode. Clearly, the timescales of the non-oscillatory modes are similar to the timescale of the oscillatory mode, and we may expect to find some interaction between the various modes. Further information is again given by the eigenvectors, which indicate that the non-oscillatory modes involve significant interactions between all of the state variables

(Table 9). In the divergence mode an increase in pitch angle ($\delta\theta>0$) is accompanied by a decrease in forward velocity ($\delta u<0$), which leads to a stall following a nose-up disturbance and a nosedive following a nose-down disturbance. This is not dissimilar to a divergent motion that appears to limit the length of glides in *Locusta migratoria* (Baker and Cooter, 1979). These are begun at a positive pitch angle (typically 15–20°), but end at a negative pitch (as low as –30°). Stable flight is only recovered when flapping is reinitiated. This rotation takes place over about 0.25 s, which identifies a divergent mode operating on a similarly short timescale to the mode we have identified.

In both the subsidence and divergence modes, changes in pitch rate (δq) are small relative to changes in pitch attitude ($\delta\theta$), whereas changes in forward velocity (δu) are comparatively large. This implies significant coupling of speed and pitch, as already shown by the strong negative relationship found between pitching moment and tunnel speed. This kind of coupling does not occur in fixed wing aircraft (in which the speed derivative M_u is close to zero at subsonic speeds), but does occur in helicopters as a result of the positive pitching moments induced as the rotor 'flaps' back with increasing speed (e.g. Padfield, 1996). This leads to mildly unstable longitudinal dynamics in helicopters, and it therefore seems likely that the speed derivative M_u may be contributing to the instability observed in the divergence mode we have identified. This is confirmed by the root locus plots of Fig. 11A–C, which illustrate the effect of systematically reducing the value of M_u to zero for each of the locusts. In each case, the positive real root becomes less positive (i.e. less unstable) as $M_u \rightarrow 0$, and in the case of locust 'R' the root is negative (i.e. stable) by the time $M_u=0$. In fact, for $M_u \approx 0$, locust 'R' is completely stable.

One surprising outcome of the eigenvector analysis is that the signs of δu and δw are switched in the subsidence mode of locust 'B' compared to the other two locusts (Table 9). We have already remarked, on the basis of the regression statistics, that the system matrix for locust 'B' is the least reliable. Comparison of the system matrices indicates that the incidence derivative X_w is considerably smaller in locust 'B' than in either of the other two locusts, and is actually non-significant in locust 'B' ($P>0.05$). Substituting the corresponding value from either of the other two locusts renders the subsidence mode eigenvector qualitatively identical to those of the other locusts. We are therefore reasonably confident that locusts 'R' and 'G' correctly identify the nature of the subsidence mode.

Error analysis

How reliable are these results? There are two components to answering this question. The first concerns the sensitivity of the results to measurement error; the second (see Discussion) concerns the effect of the various assumptions made in the course of arriving at the static system matrices. To investigate the effects of measurement error, we used the 95% confidence intervals for the partial derivatives in Table 6 to parameterize each of the six static stability derivatives as a normally distributed variable. We then ran a Monte Carlo simulation in Matlab in which the stability derivatives were varied randomly together. For the purposes of this analysis, it was assumed that the equilibrium flight speed u_e, equilibrium body angle $\alpha_{b,e}$, reference body mass m and pitching moment of inertia I_{yy} are all measured without error. This assumption is not meant literally, but is reasonable to make because errors in $\alpha_{b,e}$, m and I_{yy} will only modify the same six matrix elements that we are already varying, and variation in u_e between individuals provides a wide bracket upon the effects of errors in u_e.

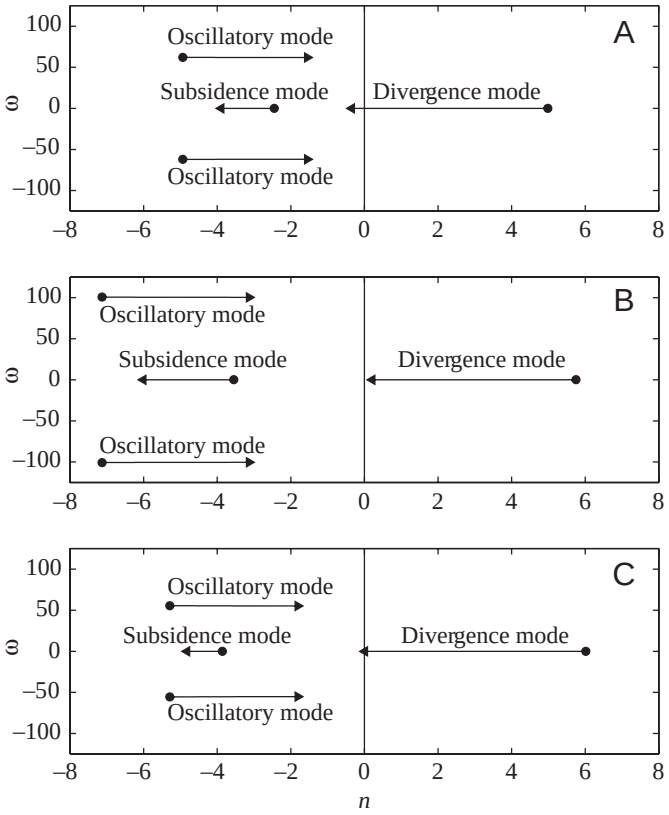

Fig. 11. Root locus plots showing the effect of reducing the speed derivative M_u to zero for each of the three locusts upon the roots of the longitudinal equations of motion. The plots are in Argand diagram form, i.e. the real part of the root (n) is plotted along the x-axis and the imaginary part of the root (ω) is plotted along the y-axis. Roots to the left of the vertical black line are stable. The filled circles denote the position of the roots of the system matrices defined in Equations 16; the centres of the triangles denote the position of the roots of the system matrices when $M_u=0$. (A) Locust 'R'. (B) Locust 'G'. (C) Locust 'B'. Note that reducing the value of M_u causes the divergence mode to move towards stability.

We ran the Monte Carlo simulation 5000 times for each locust, recalculating the eigenvalues after each iteration. The results are plotted in Argand diagram format in Fig. 12A–C, which show sufficient overlap for us to be confident that all three locusts share the same underlying flight dynamics. The plots show that the complex conjugate roots (represented by the clouds of points for which $\omega \neq 0$) are stable (i.e. ($n<0$) in 100% of cases for locusts 'R' and 'G', and are stable in 99.9% of cases for locust 'B'. The conclusion that the static stability

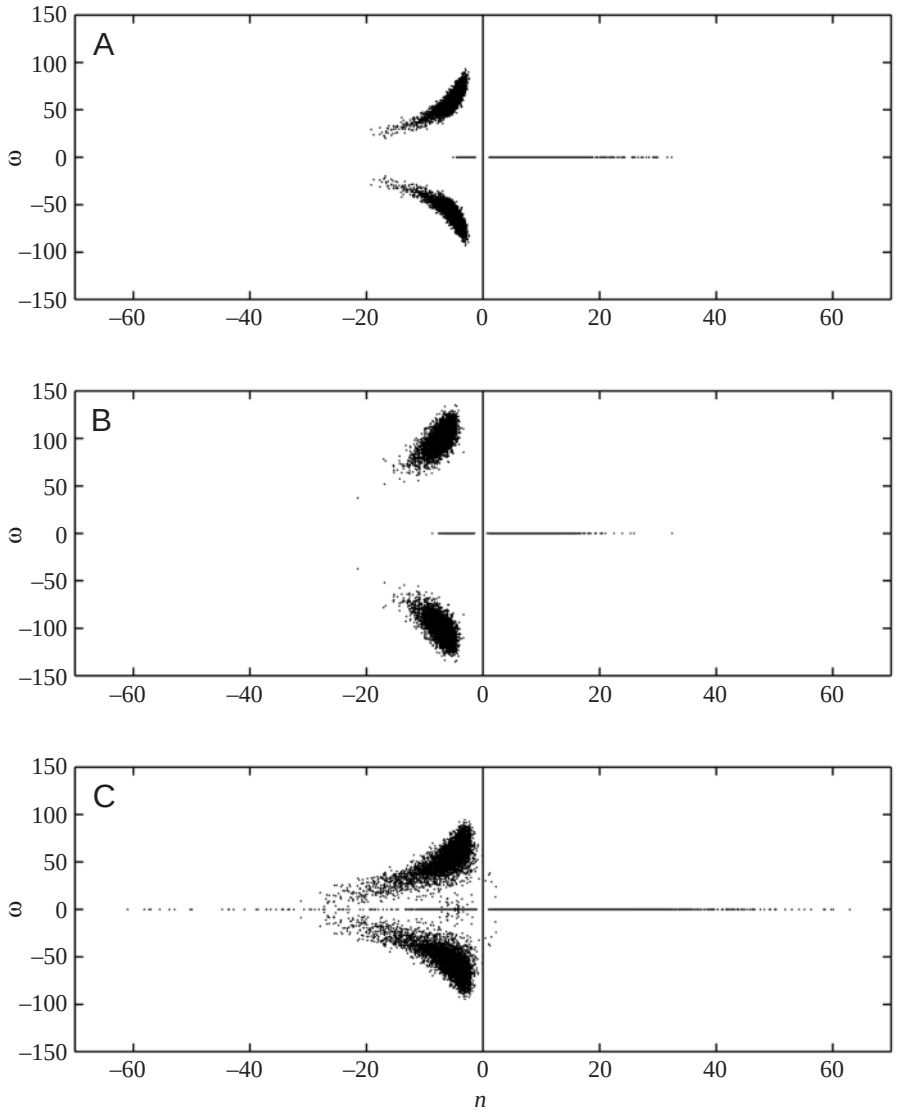

Fig. 12. Results of a Monte Carlo simulation in which the six static stability derivatives were allowed to vary as normally distributed variables, according to the parameters set by the regression analyses. The analysis was repeated 5000 times for each locust, recalculating the eigenvalues after each iteration. Each Argand diagram plot contains 20 000 points: 5000 for each of the four roots. (A) Locust 'R'. (B) Locust 'G'. (C) Locust 'B'. The plots show that the complex conjugate roots (represented by the clouds of points for which $\omega \neq 0$) are stable (i.e. $n<0$) in 100% of cases for locusts 'R' and 'G', and are stable in 99.9% of cases for locust 'B'. There are two real roots, one positive and one negative, in 100% of cases.

derivatives imply the existence of a single, damped oscillatory mode of motion is therefore robust within the bounds of experimental error. The results also show that there are two real roots – 1 positive and 1 negative – in 100% of cases. The conclusion that the static stability derivatives of locusts are insufficient to confer complete dynamic stability is therefore also robust within the bounds of experimental error.

Discussion

Failure of the model to explain dynamic stability in locusts

Although none of the locusts appears to have flown in a state corresponding to complete free-flight equilibrium, all three locusts produced near-equilibrium levels of lift under certain flight conditions. Flight performance was very consistent over the 13 s of each measurement, and the pairing of the angle series analysis did an excellent job of removing spontaneous variations in flight performance from one measurement to the next. At least two of the locusts experienced pitch equilibrium at some point during the experiments, and 1 also experienced equilibrium levels of thrust–drag production. This is arguably an advance upon previous work with tethered locusts, since no previous study has attempted to determine whether or not the locusts were at pitch equilibrium. Moreover, in some previous studies, the locusts failed to lift their own body weight (Gewecke, 1975). The mean relative thrust–drag produced by locusts 'R' and 'B' during the angle series (mean T_r=0.95) corresponds to a free flight forward acceleration of approximately 9.4 m s^{-2}. This is far from equilibrium, but well within the range of free flight forward accelerations measured in several species of large dragonfly: up to 27.8 m s^{-2} for *Macromia taeniolata* (May, 1991); up to 15.1 m s^{-2} for *Anax junius* (May, 1991); up to 13 m s^{-2} for *Aeschna cyanea* (Rüppell, 1989). Such accelerations are not unexpected in tethered flight at tunnel speeds slower than the preferred flight speed. The generally much lower levels of relative thrust production in locust 'G' (compare especially Fig. 7G–I) probably reflect its smaller size (Table 1), and may indicate that it was flying nearer to its preferred flight speed.

Assuming the locusts were flying acceptably close to equilibrium, the measured static stability derivatives are sufficient to confer static stability with respect to speed and pitch, but insufficient to confer complete dynamic stability. Since all of the locusts were capable of stable free flight, the analysis we have presented so far must therefore be deficient in some way. There are five major ways in which the analysis could be deficient, and these may be ranked in hierarchical fashion according to the point at which the analysis fails. It makes best sense to work backwards – that is to consider deficiencies entering at a later stage of the analysis first.

1. The static stability derivatives that we have measured may be somehow unrepresentative of natural free flight

The experimental conditions used are not a literal open-loop

version of the conditions experienced by a free-flying locust. Most significantly, the locusts lacked any optic flow to simulate steady progression through the environment visually. We do not consider this to be a likely source of the observed instability, because locusts commonly fly at altitude or in twilight, when there is little or no optic flow. However, it is possible that the locusts would have perceived some of the nearby objects as fixed, which is quite different to there being no optic flow and might produce unusual flight behaviour. It is also possible that the locusts were attempting take-off from the force balance, and were therefore intentionally inducing a divergence mode, but this also seems unlikely given that the complete flight posture they were using is not adopted during take-off.

2. It is erroneous to conflate w *and* θ *in determining the stability derivatives if the locusts possess a static sense of pitch attitude*

In an aircraft, passive stability arises through changes in the flow around the wings and body. This means that wind tunnel measurements of the passive aerodynamic stability derivatives of a model aircraft can be made just as well with the model upside down as with the model the right way up, provided the aerodynamic incidence is the same (e.g. Barlow et al., 1999). It follows that the forces and moments generated by an automatic control system could also be characterised with the model inverted if the control settings were linked only to aerodynamic instruments. This equivalence would of course cease to apply if the controls were linked to instruments sensing pitch attitude with respect to the ground. Framed in this way, the difference between pitch attitude and aerodynamic incidence control seems rather obvious. What may be less obvious is the corollary that nervous control mechanisms linked to changes in pitch attitude (measured relative to an inertial frame) are not dynamically equivalent to nervous control mechanisms linked to aerodynamic incidence or body angle (measured relative to the direction of flight).

Consider the phugoid motion of an aircraft. In this mode, large changes in pitch attitude are accompanied by relatively insignificant changes in aerodynamic incidence. Since the static pitch stability built into most aircraft derives from the derivative M_α, which in turn derives from the incidence derivative M_w (Equation 15), static pitch stability has rather little effect upon the damping of the phugoid. By contrast, the short period mode does involve significant changes in incidence, and is therefore heavily damped in any aircraft in which M_α is large and negative. An automatic control system linked to aerodynamic incidence is therefore only effective at providing damping of the short period mode of motion. On the other hand, since the phugoid and short period modes both involve large changes in pitch attitude, both modes of motion are effectively damped by a control mechanism linked to pitch attitude. In fact, just such mechanism is usually present in aircraft autopilots, in which it is linked to the vertical gyro (e.g. Etkin and Reid, 1996).

In the analysis we have presented so far, we have not distinguished between changes in the forces and moments due to aerodynamic incidence and changes in the forces and moments due to pitch attitude. Pitch attitude is measured with respect to inertial space, which for the purposes of this analysis is fixed with respect to both gravity and the horizon. It follows that visual or gravimetric input could provide the necessary reference for pitch attitude control in flying animals. Separating pitch attitude control from aerodynamic incidence control experimentally would therefore require a more complex arrangement in which the airstream could be rotated relative to an Earth-fixed visual frame of reference. A much simpler alternative is to simulate the effect of introducing pitch attitude control mathematically by introducing a new derivative M_θ into the system matrix.

If locusts do use pitch attitude control, the derivative that we have thus far characterised as M_α will include elements due to both M_θ and M_w. Assuming these combine additively (which follows from the linearization of this analysis), we may

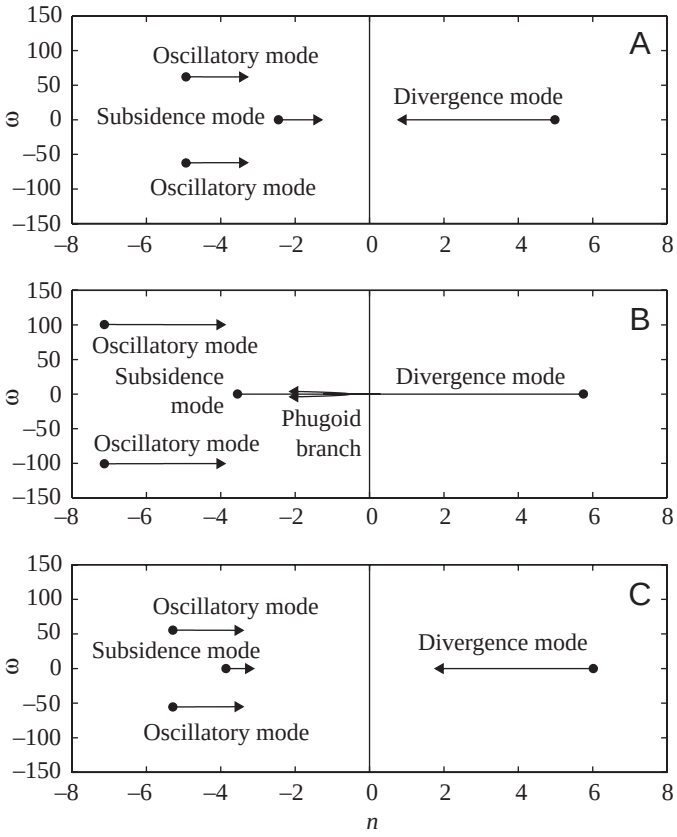

Fig. 13. Root locus plots showing the effect of partitioning the static stability derivative M_α into components due to pitch attitude (M_θ) and aerodynamic incidence (M_w). Symbols and axes are as in Fig. 11. All additive combinations of M_θ and M_w that are compatible with the measured values of M_α are shown. Note that the positive real root part of the unstable divergence mode becomes strikingly less positive (i.e. less unstable) as the ratio of M_w to M_θ tends toward zero. (A) Locust 'R'. (B) Locust 'G'. (C) Locust 'B'. In the case of locust 'G' the two real roots eventually converge and split into a complex conjugate pair, corresponding to the phugoid mode of aircraft.

therefore partition M_α into components due to aerodynamic incidence and pitch angle. The root locus plots of Fig. 13 show all of the possible additive combinations of M_θ and M_w that are compatible with the values of M_α measured for each of the three locusts. The damping of the short period mode decreases a little as the ratio of M_w to M_θ tends towards zero, but the mode remains stable. By contrast, the positive real root part of the unstable divergence mode becomes strikingly less positive (i.e. less unstable) as the ratio of M_w to M_θ tends toward zero. In the case of locust 'G' there comes a point at which the real parts of all the roots are negative (i.e. completely stable). Beyond this point the two real roots converge and split into a complex conjugate pair of long period (1.72 s) that resembles the phugoid mode of aircraft. The two real roots of locusts 'R' and 'B' also converge if the pitch attitude damping is made sufficiently large, although this is not compatible with the measured values of M_α. This analysis therefore indicates that pitch attitude control could be critical in stabilising locust flight.

Pitch attitude control has received little attention in the locust flight literature, but there is some evidence to suggest that locusts are sensitive to pitch attitude. For example, locusts are known to pitch their heads in response to pitching of an artificial horizon (Taylor, 1981a), and whilst nothing direct is known about the accompanying changes in aerodynamic force production, head movements are known to be closely associated with turning about the roll and yaw axes (e.g. Goodman, 1965; Camhi, 1970; Cooter, 1979; Taylor, 1981a,b; Robert and Rowell, 1992a,b). It was not possible to make sufficiently accurate measurements from the video recordings to determine whether the locusts displayed similar head movements in this study. Diffuse overhead illumination such as we used in this study ought, however, to be sufficient to elicit a pitch attitude response (Taylor, 1981b; *contra* Zarnack and Möhl, 1977), because the pitching movements of the head are mediated by an ocellar response (Taylor, 1981a). This is presumably based upon changes in the relative stimulation of the median ocellus and lateral ocelli (Rowell, 1988), but it is likely that the compound eyes might also play some role in detecting pitch disturbances. It is therefore possible that brighter lighting conditions than we used would have elicited a stronger response to changes in pitch.

3. The dropped rate derivatives may be important

Since we were only able to measure static stability derivatives, rate derivatives were dropped at an early stage of the analysis. Dropping the rate derivatives does not in general lead to a loss of stability in aircraft. This is clearly shown by Table 10, which compares the characteristic roots of the complete and static system matrices for a Navion NA-154 light aircraft (calculated from data in Nelson, 1989). The real parts of the roots are negative in both cases, indicating that on a simple yes/no assessment, the stability of the system is unchanged. In general, the static system matrix gives a surprisingly good first approximation to the behaviour of the system: only the damping of the short period mode is significantly affected by dropping the rate derivatives.

Physically, the reason why only the damping of the short period mode is strongly affected by the rate derivatives is that significant linear and angular accelerations are only experienced during rapid motions. Even a high degree of rate damping will have little effect upon a slow motion like the phugoid, so pitch rate damping should not greatly affect

Table 10. *Characteristic roots, or eigenvalues, of the complete and static system matrices for the NA-154 Navion light aircraft*

	Eigenvalues	
System matrix	Phugoid	Short period
Complete	–0.017±0.21*i*	–2.4±2.5*i*
Static	–0.014±0.26*i*	–1.0±2.7*i*

Calculated from data in Nelson (1989).

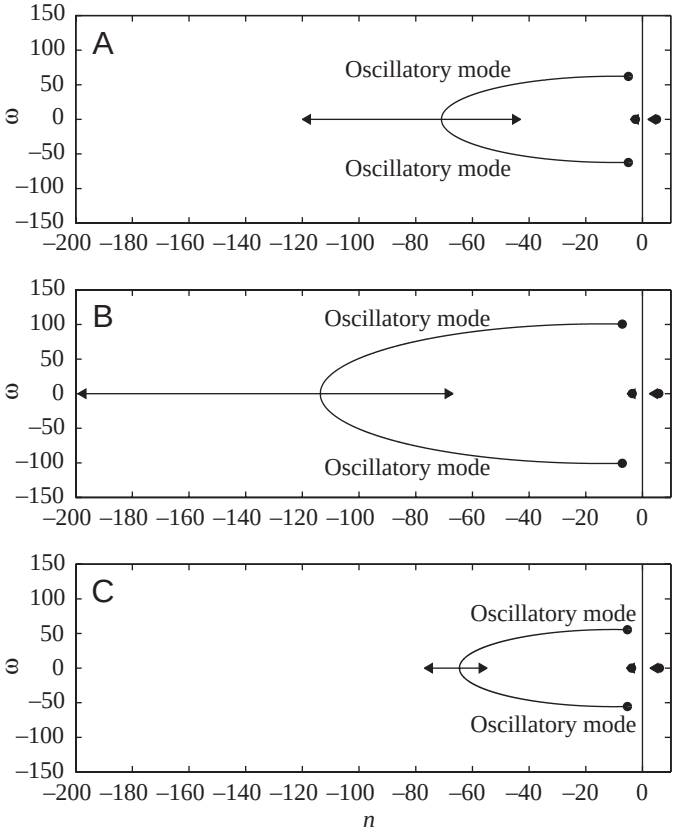

Fig. 14. Root locus plots showing the effect of introducing pitch rate damping by increasing the value of the pitch rate derivative M_q from zero. Symbols and axes are as in Fig. 11. (A) Locust 'R'. (B) Locust 'G'. (C) Locust 'B'. Increasing M_q has practically no effect upon the non-oscillatory modes, but causes the short period oscillatory mode to become more heavily damped. Eventually, critical damping is reached and the complex conjugate roots split into two negative real roots. The short period mode becomes non-oscillatory when the ratio M_q:M_α is 0.035 in locust 'R', 0.021 in locust 'G', and 0.040 in locust 'B'.

damping of the unstable divergence mode in locusts. This prediction is borne out by the root locus plots of Fig. 14, which illustrate the effects of introducing pitch rate damping into the system matrix by increasing the value of the most important rate derivative, M_q, from zero. Increasing M_q has practically no effect upon the non-oscillatory modes, so we are reasonably confident that dropping the rate derivatives has not generated the instability that we have identified. By contrast, the short period oscillatory mode becomes much more heavily damped as M_q is increased. Eventually, critical damping is reached and the complex conjugate roots split into two negative real roots. This suggests that pitch rate damping could be important in damping out the short period mode in locusts, as even a moderate degree of pitch rate damping is sufficient to suppress the oscillations completely.

In quantitative terms, the short period mode becomes non-oscillatory when pitch rate damping is introduced such that the ratio M_q:M_α is 0.035 in locust 'R', 0.021 in locust 'G', and 0.040 in locust 'B'. For a Boeing 747 cruising at 12 200 m, this ratio is approximately 0.242 (Etkin and Reid, 1996). Physically, the effects of a given degree of pitch rate damping (as measured by the ratio M_q:M_α) are more pronounced at smaller size because of the larger angular accelerations associated with the intrinsically shorter timescales of the characteristic modes of motion. Some degree of pitch rate damping of the short period mode may therefore be essential in stabilising locust flight, and possibly insect flight in general. This is because the natural frequency of the short period mode is only half that of the wingbeat, which makes it likely that the flapping cycle would couple with the short period mode if the latter were not adequately damped.

Electrophysiological evidence suggests that locusts are sensitive to pitch rate (Möhl and Zarnack, 1977), although it is not clear which sensory system provides the input for this response. Pitch rate sense has only been discussed in any detail for flies (Diptera). In flies, angular velocity is detected about all three orthogonal axes by the highly non-orthogonal halteres (Nalbach, 1993, 1994; Nalbach and Hengstenberg, 1994). The stimulus for this response is the Coriolis force experienced by the beating halteres during turning (Nalbach, 1993). Interestingly, the non-orthogonality of the halteres results in enhanced sensitivity for pitch compared to roll (Nalbach, 1994), and it is possible that this relates to the importance of pitch rate damping in providing adequate damping of the short period mode in the face of excitation by the flapping cycle.

Coupling of the short period mode with the flapping cycle could lead to catastrophic flight handling problems for the locust, which begs the question of why it should want to have a mode of motion so close to the flapping cycle in frequency. Much the same problem arises in aircraft, where the frequency of the short period mode is usually similar to the human pilot's own response time (Cook, 1997). Adequate damping of the mode is therefore essential in avoiding pilot-induced oscillations. Nevertheless, for the aircraft to display good handling qualities, it is essential for the short period mode to have a frequency close to the pilot's response time.

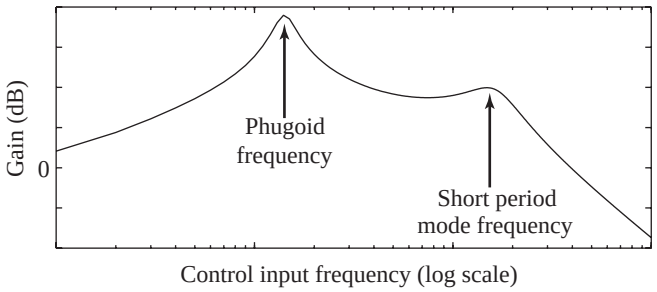

Fig. 15. Classical form of the frequency–response curve of an aircraft, illustrating the effect of making a sinusoidal control input to the elevator. The graph plots how the ratio of the output (in this case, pitch attitude θ) to input (in this case, elevator angle) varies with the frequency of the control input. The gain is plotted in decibels and the control input frequency is plotted on a logarithmic scale. The graph indicates that the gain peaks (due to resonance effects) when the control input frequency coincides with the natural frequencies of the natural modes of motion. The gain drops off sharply at control input frequencies higher than the natural frequency of the short period mode, which therefore limits the bandwidth of the aircraft's frequency response. In insects, control inputs made at the level of a single wingbeat will not be effective if the wingbeat frequency is much greater than the natural frequency of the short period mode.

At low forcing frequencies, all of the state variables show a clear sinusoidal response to a sinusoidal control input. Although control inputs are rarely purely sinusoidal in aircraft, an arbitrary waveform can be represented as a summation of sinusoids of varying amplitude and phase. The same principle applies in flapping flight, because control inputs will generally be harmonics of the wingbeat frequency. As the forcing frequency is increased, inertia will prevent an aircraft from responding quickly enough to follow the input, so the response of the state variables will lag behind the control input. At the same time, the amplitude of the sinusoidal response will diminish, eventually becoming imperceptible at a frequency corresponding to the bandwidth of the aircraft's frequency response. Effectively, the aircraft acts like a low-pass filter to the control inputs applied to it. The same will be true of flying animals, and this is clearly of relevance to understanding the evolution of their neuromuscular control systems.

A generalised plot of an aircraft's frequency response looks something like the pitch attitude gain response illustrated in Fig. 15, with clear peaks in the response of the aircraft to pilot inputs made at the frequencies of the natural modes of motion. At forcing frequencies close to the phugoid frequency, the aircraft behaves as an amplifier and relatively small control inputs lead to large amplitude responses in the state variables. The gain is usually smaller at the frequency of the short period mode because the short period mode is more heavily damped than the phugoid. It follows that the pitch attitude bandwidth frequency is usually only a little higher than the frequency of the short period mode. This means that whilst it would be undesirable for an oscillatory mode of motion to coincide exactly with the flapping cycle, its frequency should be only a

little less than the wingbeat frequency (and certainly of the same order of magnitude) if control inputs made at the level of a single wingbeat are to be effective in controlling the animal's flight.

4. A linear model may be inadequate to describe this system

"*It is almost invariably true to say that behind a linear system is a non-linear one to which it is intended to be an approximation*" (Power and Simpson, 1978). With this principle in mind we note that the issue we must address here is not whether locust flight is a linear phenomenon, which it certainly is not, but whether the linearized approximations are sufficient to capture the essentials of the system's behaviour. It is reassuring that the aerodynamic forces and moments are well modelled as linear functions of speed and angle of attack perturbations when one or other of these variables is held constant and the other is varied. In a rigid aerodynamic system this would be sufficient to imply that changes in speed and incidence should also combine additively in their effects. This will not necessarily hold true in a controlled system, however, because there is no guarantee that a locust will respond in the same way to a given pitch disturbance at different speeds.

Such interactions would clearly violate the assumption of linearity and would greatly complicate the required analysis if the non-linear effects were significant. Interaction effects could be either stabilising or destabilising in their effects, so it is possible that their neglect could explain the instability of the linear model. For example, since an increase in θ is accompanied by an increase in u and a decrease in w in the stable subsidence mode, but by opposite changes in u and w in the unstable divergence mode, it might be possible to stabilise the latter by building into the system appropriate interactions of the control responses to u, w and θ. Other forms of non-linearity such as aeroelastic hysteresis or control hysteresis are likely to promote instability, so neglecting them here is unlikely to have been the cause of instability in the system.

It is also important to note that the small disturbance equations of motion are only linear time-invariant with respect to disturbances from the equilibrium condition about which the equations are linearized. Since flight equilibrium was never attained experimentally, and since it was not possible to calculate a unique condition in which all three conditions for flight equilibrium were exactly satisfied simultaneously, the equations of motion are not strictly linear time-invariant. In this case the entries in the system matrix are (real) functions of time and it is no longer a sufficient condition for asymptotic stability that the eigenvalues of the system matrix have negative real parts for all time $t \geq 0$ (e.g. Hahn, 1967). Nevertheless, we were able to calculate a mean pseudo-equilibrium for each locust that was close to being an exact equilibrium (Table 5), and on the assumption that the empirical regression slopes would have been the same had perturbations been made from this mean pseudo-equilibrium instead of the reference flight condition, it is reasonable to treat the equations of motion as linear time-invariant.

5. The rigid body approximation may be inappropriate

We have discussed the constraints upon treating periodic variables as time-averaged constants in detail elsewhere (Taylor and Thomas, 2002). In general, this rigid body approximation only works well if the lowest frequency of the periodic variables is at least an order of magnitude higher than the highest frequency of the natural modes of motion. We previously reasoned (Taylor and Thomas, 2002) that this could be expected to be true in animal flight, partly on the basis of approximations to the natural modes of motion and partly on the basis of the observation that resonance effects between the natural modes of motion and the flapping cycle are rarely observed. By contrast, the analysis here identifies a short period mode of motion whose frequency is only half that of the wingbeat frequency, and we have already said that the flapping cycle is therefore liable to excite the short period mode. How can we explain this discrepancy?

The reduced-order approximation that we used to approximate the period of the short period mode previously (Taylor and Thomas, 2002) was:

$$T \approx \frac{2\pi}{\sqrt{-M_\alpha / I_{yy}}} . \quad (26)$$

This identifies a constrained pitching motion of period T_R=0.10 s, T_G=0.06 s, T_B=0.11 s for the three locusts. These periods are identical to the periods obtained through the eigenvalue analysis at the level of precision shown, although the two compare so favourably principally because we used a static system matrix in the analysis. Nevertheless, this is another good confirmation that the oscillatory mode we have identified corresponds to the short period pitching mode of aircraft. The discrepancy with our previous analysis (Taylor and Thomas, 2002) arises because there we did not discuss allometry in the scaling of M_α and I_{yy}.

Specifically, because M_α scales as the product of a force and a length, it scales with the fourth power of the linear dimensions. On the other hand, because I_{yy} scales as the product of mass and area, it scales as the fifth power of the linear dimensions. Other things being equal, the period of the short period mode should therefore scale as the square root of the linear dimensions. This is why the short period mode is much closer in frequency to the stroke cycle than we had previously predicted (Taylor and Thomas, 2002). It follows that the rigid body approximation is only likely to be valid in flapping flight if the pitch rate damping is sufficiently high that the flapping cycle does not normally excite the short period mode. Equations of motion have recently been derived that include three rotational degrees of freedom for each of two flapping wings (Gebert et al., 2002), so the theoretical framework now exists for future experimental work to take account of the wing motions.

General conclusions

Earlier work on the longitudinal flight mechanics of locusts has been dominated by analysis of an influential paradigm: the

so-called ‘constant-lift reaction’ (Wilson and Weis-Fogh, 1962), in which locusts are supposed to produce the same vertical force across a 20° range of body angles (Weis-Fogh, 1956a,b; Gewecke, 1975). The ‘constant-lift reaction’ is supposed to result from a consistent and well-known response to imposed changes in pitch, whereby forewing inclination adjusts to compensate for the disturbance (Gettrup and Wilson, 1964; Gettrup, 1966; Wortmann and Zarnack, 1993; Fischer and Kutsch, 2000) under active muscular control (Wilson and Weis-Fogh, 1962; Gettrup, 1966; Zarnack and Möhl, 1977). Because hindwing inclination remains unchanged with respect to the body (Gettrup and Wilson, 1964; Wortmann and Zarnack, 1993), the lift on the hindwings would be expected to increase with increasing body angle, but this is supposed to be compensated for by a drop in flight speed (Gettrup and Wilson, 1964), resulting in the maintenance of approximately constant lift.

Remarkably, no study of the ‘constant-lift reaction’ has ever measured the pitching moments associated with changes in body angle, so it has not been possible to say whether free-flying locusts would remain at perturbed angles long enough for a ‘constant-lift reaction’ to have any noticeable effect. The high frequency of the stable short period mode indicates that angle of attack disturbances would be corrected for rather quickly in stable free flight. A ‘constant-lift reaction’ would therefore be inconsequential because the locust would correct its body angle within a single wingbeat, assuming critical damping of the short period mode. The same changes in forewing kinematics that have been implicated in the ‘constant-lift reaction’ will tend to shift the balance of lift between fore- and hindwings so as to generate a stabilising pitching moment, and are probably responsible for the static pitch stability of locusts (Wilson and Weis-Fogh, 1962; Gettrup and Wilson, 1964; Taylor, 2001). This may also explain why body angle disturbances are corrected within a time period almost identical to that of a single wingbeat. Given that more recent experiments (Zarnack and Wortmann, 1989; Wortmann and Zarnack, 1993) contradict the observations upon which the ‘constant-lift reaction’ is premised, and are consistent with the force measurements in this study, it seems that we may firmly reject the ‘constant-lift reaction’ hypothesis.

The case of the ‘constant-lift reaction’ is instructive because the hypothesis is predicated upon an oversimplification of the dynamics of flying bodies. As we have shown, all of the longitudinal state variables are coupled in some way, which means that the response to an apparently straightforward control input is far from simple. For example, in aircraft a step increase in the throttle results in an immediate increase in flight speed, as intuition would suggest. However, if the thrust line passes through the centre of mass, this increase in speed excites a damped phugoid oscillation, which converges towards a steady state in which the flight speed is unchanged from its initial value but in which the flight path is tilted up from the initial line of flight! We would strongly caution against making any conclusions about the dynamic effects of measured insect control responses without performing a dynamic analysis similar to that we have used here.

We have argued above that the frequency of the short period mode of motion will need to be close to the wingbeat frequency for an insect to be able to control its flight with control inputs made at the level of a single wingbeat. Similar considerations will apply in birds, but they are arguably less constrained than insects in this respect because the tail provides a control surface that can be operated at timescales not dictated by the wingbeat frequency. In insects, size-dependent scaling of the short period mode frequency will have important consequences for the frequencies at which the neuromuscular system must operate. Control inputs made at frequencies much higher than the short period mode frequency will be ineffective, and for maximum efficiency we would expect the control responses of the nervous system to be tuned to approximately this frequency. We therefore predict that for insects of similar morphology but differing size, the intrinsic timescales at which the neuromuscular control system should operate will scale as the square root of the insect’s linear dimensions. The intrinsic frequencies of the neuromuscular control system should therefore scale as one over the square root of the linear dimensions.

The frequency of the short period mode is a function of the pitching moment of inertia. The effect on this of adding body mass is proportional to the square of the distance to the centre of mass from the point at which the mass is added. If locusts were compensating for this perfectly by putting less body mass towards the extremities then we would expect the bar graph of the percentage contributions of different body sections to the total pitching moment of inertia (Fig. 5D) to be flat. It is not: the bar graph of the percentage contributions to the total pitching moment of inertia (Fig. 5D) mirrors almost perfectly the bar graph of the percentage contributions of different body sections to total body mass in the three locusts (Fig. 5A), which is anything but flat. This indicates that locusts are under-compensating for the increasing cost of adding mass towards the extremities, and hints at strong functional constraints in body shape and mass distribution. For example, the head is by far the most costly section in terms of its contribution to the total pitching moment of inertia, even though it lies much closer to the centre of mass than many parts of the abdomen. This is presumably because the organs that it houses (eyes, brain, mouthparts) are some of the most important, their localisation in the body is crucial, and they are rather strictly limited in size to being above some useful minimum.

Because the frequency of the short period mode is a function of the mass distribution of the insect, body shape is crucial in determining an insect’s frequency response. For example, the elongate body forms associated with more primitive groups of insect would tend to confer a narrower bandwidth and hence a poorer frequency response. This would constrain manoeuvrability, but would be preferable to having a wider bandwidth that would couple the short period mode and the flapping cycle in the absence of a highly evolved control system to provide pitch rate damping.

Conversely, shortening of the abdomen tends to be associated with greater manoeuvrability: darter dragonflies and hoverflies are prominent examples of this. Although the conclusion that insects should reduce their moments of inertia to enhance manoeuvrability is old news, we have shown for the first time that mass distribution should be linked in predictable ways to wingbeat frequency, flight morphology and the response characteristics of the nervous system itself. Flight dynamics therefore provides a formal quantitative framework by which to unite the fields of flight mechanics and neurophysiology.

On the value of true open-loop studies

It has been argued previously (Weis-Fogh, 1956a) that allowing tethered insects to indirectly control wind tunnel speed simulates flight more naturally than if the tunnel speed is held fixed. Whilst there is certainly some logic in this argument, it must be stressed that the conditions that this produces remain highly artificial unless body angle is also allowed to vary freely. Even though body angle was allowed to vary in some of Weis-Fogh's experiments (Weis-Fogh, 1956a), the axis of rotation was not aligned with the centre of mass, which would, in any case, have been affected by the mounting. Unless there are clear reasons for doing otherwise, we think it preferable to vary only one degree of freedom at a time, thereby preserving true open-loop conditions, instead of using a hybrid system that closes some control loops whilst leaving others open. In the present case, this means holding tunnel speed fixed whilst body angle is varied, and *vice versa*.

Although there are some disadvantages to this scheme (for example, it may be difficult to determine whether the animals are flying at their preferred flight speed prior to analysing the data), using true open-loop conditions removes many possible ambiguities in interpreting experimental results. Results from free-flying locusts described above notwithstanding (Baker et al., 1981), flight speed and body angle do appear to be negatively correlated in many insects (for a review, see Taylor, 2001). The same is true of helicopters and fixed-wing aircraft. The observed closed-loop changes in flight speed in Weis-Fogh's experiments (Weis-Fogh 1956a,b) are therefore of uncertain significance because body angle was not allowed to co-vary naturally with flight speed.

A second advantage of using true open-loop conditions is that the changes in the flight forces measured then correspond directly to the partial derivatives, or stability derivatives, that are central to the dynamic analysis that we have made here. Although our tethered force measurements were made under open-loop conditions, the quantitative framework that we have provided offers a means of simulating the closed-loop dynamics of free flight. Provided there is no hysteresis in the system, such that open-loop measurements are equivalent to a snapshot of closed-loop conditions, then open-loop measurements of the forces and moments offer a tractable point of entry into the wonderful complexities of animal flight dynamics.

List of symbols

This list contains only those symbols that appear in the main body of the paper. Symbols appearing only in the Appendix are not included.

a	total projected side area of the body
a_i	ith coefficient of a characteristic equation
$\mathbf{A}$	generic notation for an $n\times n$ matrix
b	stroke plane angle
$\mathbf{c}_{sym}$	longitudinal control state matrix
$\mathbf{C}$	generic notation for a diagonalizing matrix
$\mathbf{C}_{sym}$	longitudinal control system matrix
$\mathbf{D}$	generic notation for a diagonal $n\times n$ matrix
$\mathbf{F}_{sym}$	longitudinal system matrix
$\boldsymbol{g}$	acceleration due to gravity
i	counting index or imaginary number, $i=\sqrt{-1}$
$\mathbf{I}$	generic notation for an identity matrix
I_{yy}	total pitching moment of inertia about the y-axis
l	body length
L_r	relative lift (vertical component of aerodynamic force normalised by reference body weight)
m	reference body mass
m_b	reference body mass minus the mass of the wings
m_w	mass of one wing
M	pitching moment about the centre of mass
M_r	relative pitching moment (pitching moment about centre of mass normalised by reference body weight)
n	real part of an eigenvalue
q	pitch rate about centre of mass, $q=\dot{\theta}$
r	distance from centre of mass of a wing to its root
t	time
t_{double}	time for a divergent motion to double in amplitude
t_{half}	time for a damped motion to halve in amplitude
T	period of a motion
T_r	relative thrust–drag (forward horizontal component of aerodynamic force normalised by reference body weight)
u	forward velocity component along x-axis
U	tunnel speed
U_e	equilibrium tunnel speed
U_{ref}	reference tunnel speed ($3.50\,m\,s^{-1}$)
w	dorso-ventral velocity component along z-axis
x,z	dimensional coordinates in the body axes
$\hat{x}$, $\hat{z}$	dimensionless coordinates in the body axes, normalised by body length
$\mathbf{x}(t)$	generic notation for a state vector
$\mathbf{x}_{sym}(t)$	longitudinal state vector, $\mathbf{x}_{sym}(t)=[u\ w\ q\ \theta]^T$
X	forward component of aerodynamic force along x-axis
Z	dorso-ventral component of aerodynamic force along z-axis
α	angle between the x-axis of the stability axes and the horizontal (radians)
α_b	body angle
$\alpha_{b,ref}$	reference body angle (7°)

γ	positional angle of the wings, from *z*-axis to wing long axis
$\bar{\gamma}$	mean positional angle of the wings
ζ_R	damping ratio of an oscillatory mode of motion
θ	pitch attitude, angle of *x*-axis to horizontal
λ	generic notation for an eigenvalue, or root of a characteristic equation
σ_i	relative density of *i*th rectangle of block model of locust
φ	total stroke excursion angle
ω	angular frequency, imaginary part of a complex eigenvalue

Subscripts and prefixes

e	denotes a value of a variable at equilibrium
ref	denotes a reference value of a variable under reference flight conditions
sym	denotes symmetric motions
R, G, B	denote a value measured for locust 'R', 'G', or 'B', respectively
δ	small disturbance notation (prefixed to a perturbed state variable)

Stability derivatives

The following shorthand notation is used to denote a partial derivative with respect to the variable contained in the subscript.

X_q, Z_q, M_q	pitch rate derivatives
X_u, Z_u, M_u	speed derivatives
X_w, Z_w, M_w	incidence derivatives
M_θ	pitch attitude derivative
M_α	angle of attack derivative

Appendix

Development of the linearized equations of motion

In the present context, there is little to be gained from deriving the equations of motion from first principles. The reader is referred to Etkin and Reid (1996) and Boiffier (1998) for recent treatments of the subject. At the scales we are considering, it will be satisfactory to assume that gravitational acceleration ($\boldsymbol{g}$) and air density are constants and that the Earth's surface is flat and fixed in inertial space. In addition, we will assume that there is no wind, and that the animal is a rigid body with six degrees of freedom and perfect bilateral symmetry.

The nonlinear equations of motion of such a body may be written in the state vector form:

$$\dot{\mathbf{x}} = \mathbf{F}(\mathbf{x}, \mathbf{c}, t) , \tag{A1}$$

where t is time. The control vector $\mathbf{c}$ has as many elements as the animal has control degrees of freedom (see Taylor, 2001), and

$$\mathbf{x} = [u, w, q, \theta, v, p, r, \phi, \psi]^T \tag{A2}$$

is the state vector, where the superscript T denotes the transpose of the row vector shown. The translational velocity components (u, v, w) and angular velocity components (p, q, r) are defined in a right-handed system of three orthogonal axes (x, y, z, respectively) originating at the centre of mass (see Fig. 2, where the y-axis points into the page). A system of Euler angles defines the orientation of the body relative to the Earth, and is specified by the angles of right-handed rotation about the three axes in the order z (yaw, ψ), then y (pitch, θ), then x (roll, ϕ). These definitions of the state variables and forces and moments follow current American Institute of Aeronautics and Astronautics (AIAA) recommended practice (AIAA, 1992), based on International Organization for Standardization (ISO) standard 1151.

Equation A1 may be expanded as a set of nine coupled nonlinear ordinary differential equations incorporating the aerodynamic forces (X, Y, Z) and moments (L, M, N) acting along or about the body axes (e.g. Etkin and Reid, 1996; Padfield, 1996):

$$\dot{u} = -(wq - vr) + \frac{X}{m} - \boldsymbol{g}\sin\theta \tag{A3a}$$

$$\dot{v} = -(ur - wp) + \frac{Y}{m} + \boldsymbol{g}\cos\theta\sin\phi \tag{A3b}$$

$$\dot{w} = -(vp - uq) + \frac{Z}{m} + \boldsymbol{g}\cos\theta\cos\phi , \tag{A3c}$$

$$I_{xx}\dot{p} - I_{xz}\dot{r} = (I_{yy} - I_{zz})qr + I_{xz}pq + L \tag{A4a}$$

$$I_{yy}\dot{q} = (I_{zz} - I_{xx})pr + I_{xz}(r^2 - p^2) + M \tag{A4b}$$

$$I_{zz}\dot{r} - I_{xz}\dot{p} = (I_{xx} - I_{yy})pq - I_{xz}qr + N , \tag{A4c}$$

and

$$\dot{\phi} = p + q\sin\phi\tan\theta + r\cos\phi\tan\theta \tag{A5a}$$

$$\dot{\theta} = q\cos\phi - r\sin\phi \tag{A5b}$$

$$\dot{\psi} = q\sin\phi\sec\theta + r\cos\phi\sec\theta , \tag{A5c}$$

in which I_{xx}, I_{yy} and I_{zz} are moments of inertia about the body axes and I_{xz} is the only non-zero product of inertia.

Equations A3–A5 offer little insight in their present form, but are readily linearized using small perturbation theory, which assumes that the animal's motion consists of small disturbances from a reference flight condition of steady motion. In general we have:

$$\mathbf{x} = \mathbf{x}_e + \delta\mathbf{x} , \tag{A6}$$

where the subscript e (for equilibrium) denotes the reference flight condition, and the prefix δ denotes a small disturbance quantity. For simplicity, the reference flight condition is assumed to be symmetric with no angular velocity. Hence,

$$v_e = p_e = q_e = r_e = \phi_e = 0 , \tag{A7}$$

and therefore

$$v = \delta v,\ p = \delta p,\ q = \delta q,\ r = \delta r,\ \ \phi = \delta\phi\ . \qquad \text{(A8)}$$

If the following trigonometric approximations are also used:

$$\sin(\theta_e + \delta\theta) \approx \sin\theta_e + \delta\theta\cos\theta_e$$

$$\cos(\theta_e + \delta\theta) \approx \cos\theta_e - \delta\theta\sin\theta_e$$

$$\tan(\theta_e + \delta\theta) \approx \tan\theta_e$$

$$\sec(\theta_e + \delta\theta) \approx \sec\theta_e$$

$$\sin\phi \approx \delta\phi$$

$$\cos\phi \approx 1\ , \qquad \text{(A9)}$$

then incorporating the small disturbance notation into Equations A3–A5 and dropping any non-linear terms in the disturbance quantities, we have:

$$\delta\dot{u} = -w_e\delta q + \frac{X}{m} - \boldsymbol{g}(\sin\theta_e + \delta\theta\cos\theta_e) \qquad \text{(A10a)}$$

$$\delta\dot{v} = -u_e\delta r + w_e\delta p + \frac{Y}{m} + \boldsymbol{g}\cdot\delta\phi\cos\theta_e \qquad \text{(A10b)}$$

$$\delta\dot{w} = -u_e\delta q + \frac{Z}{m} + \boldsymbol{g}(\cos\theta_e - \delta\theta\sin\theta_e) \qquad \text{(A10c)}$$

$$I_{xx}\delta\dot{p} - I_{xz}\delta\dot{r} = L \qquad \text{(A11a)}$$

$$I_{yy}\delta\dot{q} = M \qquad \text{(A11b)}$$

$$I_{zz}\delta\dot{r} - I_{xz}\delta\dot{p} = N\ , \qquad \text{(A11c)}$$

and

$$\delta\dot{\phi} = \delta p + \delta r\tan\theta_e \qquad \text{(A12a)}$$

$$\delta\dot{\theta} = \delta q \qquad \text{(A12b)}$$

$$\delta\dot{\psi} = \delta r\sec\theta_e\ . \qquad \text{(A12c)}$$

The next step of the linearization process requires the aerodynamic forces and moments to be represented as analytical functions of the perturbed motion variables and their derivatives. Taylor's theorem for analytical functions can then be used to approximate each of the six forces and moments as an infinite series about the reference condition, retaining only first order terms to give an expansion of the form:

$$X = X_e + \frac{\partial X}{\partial u}\,\delta u + \frac{\partial X}{\partial v}\,\delta v \ldots \frac{\partial X}{\partial c_1}\,\delta c_1 \ldots \text{etc}, \qquad \text{(A13)}$$

where the term c_1 refers to the first element of the control vector, and so on. The expansion also contains partial derivatives with respect to the rates of change of the motion and control variables through time, but we will assume that these may be neglected for the purposes of this analysis (see Discussion above).

Partial derivatives of the aerodynamic forces and moments are referred to as stability derivatives and we will hereon adopt the convention of writing the stability derivatives in the form $\partial X/\partial u = X_u$. Since we have assumed that the *xz*-plane is a plane of symmetry, changes in the longitudinal variables *u*, *w*, *q* and θ induce symmetrical changes in the forces and moments. It follows that the lateral stability derivatives with respect to the longitudinal motion variables must all be zero.

Reference values of the aerodynamic forces and moments can be replaced by setting the disturbance quantities equal to zero in Equations A10–A12, yielding:

$$X_e/m = \boldsymbol{g}\sin\theta_e$$

$$Z_e/m = -\boldsymbol{g}\cos\theta_e$$

$$Y_e = L_e = M_e = N_e = 0\ . \qquad \text{(A14)}$$

After substituting the various expansions implied by Equations A13–A14 into Equations A10–A12, and solving Equations A11a,c, the linearized equations of motion can be written in state vector form as:

$$\delta\dot{\mathbf{x}}(t) = \mathbf{A}\delta\mathbf{x}(t) + \mathbf{B}\delta\mathbf{c}(t)\ . \qquad \text{(A15)}$$

If we set $\delta v = \delta p = \delta r = \delta\phi = \delta\psi = 0$, then the lateral motion variables remain zero (Equation A8) throughout the motions described by Equation A15 (i.e. $v = p = r = 0$). The linearized equations of motion then simplify to describe the pure longitudinal motions of a symmetric body, yielding:

$$\begin{bmatrix} \delta\dot{u} \\ \delta\dot{w} \\ \delta\dot{q} \\ \delta\dot{\theta} \end{bmatrix} = \begin{bmatrix} \frac{X_u}{m} & \frac{X_w}{m} & \frac{X_q}{m} - w_e & -\boldsymbol{g}\cos\theta_e \\ \frac{Z_u}{m} & \frac{Z_w}{m} & \frac{Z_q}{m} + u_e & -\boldsymbol{g}\sin\theta_e \\ \frac{M_u}{I_{yy}} & \frac{M_w}{I_{yy}} & \frac{M_q}{I_{yy}} & 0 \\ 0 & 0 & 1 & 0 \end{bmatrix} \begin{bmatrix} \delta u \\ \delta w \\ \delta q \\ \delta\theta \end{bmatrix} + \mathbf{C}_{sym}\delta\mathbf{c}_{sym}(t)\ , \qquad \text{(A16)}$$

where $\mathbf{c}_{sym}$ contains only symmetric control inputs and $\mathbf{C}_{sym}$ is the corresponding control system matrix. Despite the several other simplifying assumptions made so far, the existence of pure longitudinal motions depends only upon the assumption that the *xz*-plane is a plane of mirror symmetry, and is not a consequence of linearizing the equations (as can be shown by inspection of the non-linear Equations A3–A5). The existence of pure lateral motions depends upon a more restrictive set of assumptions, and the decoupled equations describing them are not derived here.

We thank Rafal Zbikowski for his helpful comments on an earlier incarnation of this manuscript, and thank two anonymous referees, whose helpful and constructive comments on the final version of this manuscript were extremely useful in improving it. We particularly thank the staff of the Zoology Department workshops at Oxford, especially Tony Price and Terry Barker, for their help in

making this work possible. Steve Roberts supplied quality locusts. This work was supported by the Christopher Welch Scholarship and by BBSRC grants 43/S09380 and 43/S08664. G.K.T. is supported by a Weir Junior Research Fellowship at University College, Oxford, and by a Royal Commission for the Exhibition of 1851 Research Fellowship.

References

AIAA (1992). *AIAA Recommended Practice for Atmospheric and Space Flight Vehicle Coordinate Systems*. AIAA Standards Series R-004-1992.

Apostol, T. M. (1997). *Linear Algebra. A First Course with Applications to Differential Equations*. New York: Wiley.

Baker, P. S. (1979). The wing movements of flying locusts during steering behaviour. *J. Comp. Physiol. A* **131**, 49-58.

Baker, P. S., Gewecke, M. and Cooter, R. J. (1981). The natural flight of the migratory locust *Locusta migratoria* L. III. Wing-beat frequency, flight speed and attitude. *J. Comp. Physiol. A* **141**, 233-237.

Baker, P. S. and Cooter, R. J. (1979). The natural flight of the migratory locust, *Locusta migratoria* L. II. Gliding. *J. Comp. Physiol. A* **131**, 89-94.

Barlow, J. B., Rae, W. H. and Pope, A. (1999). *Low Speed Wind Tunnel Testing*. 3rd edition. New York: Riley.

Blondeau, J. (1981). Aerodynamic capabilities of flies, as revealed by a new technique. *J. Exp. Biol.* **92**, 155-163.

Boiffier, J.-L. (1998). *The Dynamics of Flight. The Equations*. Chichester: Wiley.

Bryson, A. E. (1994). *Control of Spacecraft and Aircraft*. Princeton: Princeton University Press.

Camhi, J. M. (1970). Yaw-correcting postural changes in locusts. *J. Exp. Biol.* **52**, 519-531.

Cloupeau, M., Devillers, J.-F. and Devezeaux, D. (1979). Direct measurements of instantaneous lift in desert locust; comparison with Jensen's experiments on detached wings. *J. Exp. Biol.* **80**, 1-15.

Cook, M. V. (1997). *Flight Dynamics: Principles*. London: Arnold.

Cooter, R. J. (1979). Visually induced yaw movements in the flying locust, *Schistocerca gregaria* (Forsk.). *J. Comp. Physiol. A* **131**, 67-78.

Deng, X., Schenato, L. and Sastry, S. (2002). Model identification and attitude control scheme for a micromechanical flying insect. In *Proceedings of the Seventh International Conference on Control, Automation, Robotics and Vision, Singapore, December 2002*, pp. 1007-1012.

Eggers, A., Preiss, R. and Gewecke, M. (1991). The optomotor yaw response of the desert locust, *Schistocerca gregaria*. *Physiol. Entomol.* **16**, 411-418.

Etkin, B. and Reid, L. D. (1996). *Dynamics of Flight: Stability and Control*. New York: Wiley.

Fischer, H. and Kutsch, W. (2000). Relationships between body mass, motor output and flight variables during free flight of juvenile and mature adult locusts, *Schistocerca gregaria*. *J. Exp. Biol.* **203**, 2723-2735.

Gebert, G., Gallmeier, P. and Evers, J. (2002). Equations of motion for flapping flight. *AIAA* **2002**, 4872.

Gettrup, E. (1966). Sensory regulation of wing twisting in locusts. *J. Exp. Biol.* **44**, 1-16.

Gettrup, E. and Wilson, D. M. (1964). The lift control reaction of flying locusts. *J. Exp. Biol.* **41**, 183-190.

Gewecke, M. (1975). The influence of the air current sense organs on the flight behaviour of *Locusta migratoria*. *J. Comp. Physiol.* **103**, 79-95.

Goodman, L. J. (1965). The role of certain optomotor reactions in regulating stability in the rolling plane during flight in the desert locust *Schistocerca gregaria*. *J. Exp. Biol.* **42**, 385-407.

Hahn, W. (1967). *Stability of Motion*. Springer Verlag: New York.

Hollick, F. S. J. (1940). The flight of the dipterous fly *Muscina stabulans* Fallén. *Phil. Trans. R. Soc. Lond. B* **230**, 357-390.

Khoury, G. A. and Gillett, J. D. (1999). *Airship Technology*. Cambridge: Cambridge University Press.

Lanchester, F. W. (1908). *Aerodenetics*. London: Constable.

May, M. L. (1991). Dragonfly flight: power requirements at high speed and acceleration. *J. Exp. Biol.* **158**, 325-342.

McCay, M. G. (2001). Aerodynamic stability and maneuvrability of the gliding frog *Polypedates dennysi*. *J. Exp. Biol.* **204**, 2817-2826.

Möhl, B. and Zarnack, W. (1977). Activity of the direct downstroke flight muscles of *Locusta migratoria* (L.) during steering behaviour in flight. II. Dynamics of the time shift and changes in the burst length. *J. Comp. Physiol. A* **118**, 235-247.

Nalbach, G. (1993). The halteres of the blowfly Calliphora. I. Kinematics and dynamics. *J. Comp. Physiol.* **173**, 293-300.

Nalbach, G. (1994). Extremely non-orthogonal axes in a sense organ for rotation: behavioural analysis of the dipteran haltere system. *Neuroscience* **61**, 149-163.

Nalbach, G. and Hengstenberg, R. (1994). The halteres of the blowfly Calliphora. II. Three-dimensional organization of compensatory reactions to real and simulated rotations. *J. Comp. Physiol. A* **175**, 695-708.

Nelson, R. C. (1989). *Flight Stability and Automatic Control*. Singapore: McGraw-Hill.

Padfield, G. D. (1996). *Helicopter Flight Dynamics*. Oxford: Blackwell Science Ltd.

Power, H. M. and Simpson, R. J. (1978). *Introduction to Dynamics and Control*. London: McGraw-Hill.

Robert, D. and Rowell, C. H. F. (1992a). Locust flight steering. I. Head movements and the organization of correctional manoeuvres. *J. Comp. Physiol. A* **171**, 41-51.

Robert, D. and Rowell, C. H. F. (1992b). Locust flight steering. II. Acoustic manoeuvres and associated head movements compared with correctional steering. *J. Comp. Physiol. A* **171**, 53-62.

Rowell, C. H. F. (1988). Mechanisms of flight steering in locusts. *Experientia* **44**, 389-395.

Rüppell, G. (1989). Kinematic analysis of symmetrical flight manoeuvres of Odonata. *J. Exp. Biol.* **144**, 13-42.

Schenato, L., Wu, W. C. and Sastry, S. (2002). Attitude control for a micromechanical flying insect via sensor output feedback. In *Proceedings of the Seventh International Conference on Control, Automation, Robotics and Vision, Singapore, December 2002*, pp. 1031-1036.

Sokal, R. R. and Rohlf, J. F. (1995). *Biometry: The Principles and Practice of Statistics in Biological Research*. New York: W. H. Freeman.

Taylor, G. K. (2001). Mechanics and aerodynamics of insect flight control. *Biol. Rev.* **76**, 449-471.

Taylor, G. K. and Thomas, A. L. R. (2002). Animal flight dynamics II. Longitudinal stability in flapping flight. *J. Theor. Biol.* **214**, 351-370.

Taylor, C. P. (1981a). Contribution of compound eyes and ocelli to steering of locusts in flight. I. Behavioural analysis. *J. Exp. Biol.* **93**, 1-18.

Taylor, C. P. (1981b). Contribution of compound eyes and ocelli to steering of locusts in flight. II. Timing changes in flight motor units. *J. Exp. Biol.* **93**, 19-31.

Thomas, A. L. R. and Taylor, G. K. (2001). Animal flight dynamics I. Stability in gliding flight. *J. Theor. Biol.* **212**, 399-424.

Thüring, D. A. (1986). Variability of motor output during flight steering in locusts. *J. Comp. Physiol. A* **158**, 653-664.

Waloff, Z. (1972). Observations on the airspeeds of freely flying locusts. *Anim. Behav.* **20**, 367-372.

Weis-Fogh, T. (1956a). Biology and physics of locust flight. II. Flight performance of the desert locust (*Schistocerca gregaria*). *Phil. Trans. R. Soc. Lond. B* **239**, 459-510.

Weis-Fogh, T. (1956b). Biology and physics of locust flight. IV. Notes on sensory mechanisms in locust flight. *Phil. Trans. R. Soc. Lond. B* **239**, 553-584.

White, F. M. (1974). *Viscous Fluid Flow*. New York: McGraw Hill.

Wilkin, P. J. (1990). The instantaneous force on a desert locust, *Schistocerca gregaria* (Orthoptera: Acrididae), flying in a wind tunnel. *J. Kansas Entomol. Soc.* **63**, 316-328.

Wilson, D. M. and Weis-Fogh, T. (1962). Patterned activity of co-ordinated motor units, studied in flying locusts. *J. Exp. Biol.* **39**, 643-667.

Wortmann, M. and Zarnack, W. (1993). Wing movements and lift regulation in the flight of desert locusts. *J. Exp. Biol.* **182**, 57-69.

Zarnack, W. and Möhl, B. (1977). Activity of the direct downstroke flight muscles of *Locusta migratoria* (L.) during steering behaviour in flight. I. Patterns of time shift. *J. Comp. Physiol. A* **118**, 215-233.

Zarnack, W. and Wortmann, M. (1989). On the so-called constant-lift reaction of migratory locusts. *J. Exp. Biol.* **147**, 111-124.